Renewable Energy 247 (2025) 123002

Contents lists available at ScienceDirect

Renewable Energy

journal homepage: www.elsevier.com/locate/renene

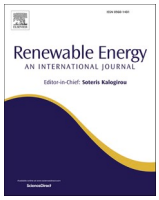

Techno-economic analysis of a renewable energy based multigeneration system for zero energy buildings

L. Aelenei *, C. Rodrigues, M.J. Brites, S. Viana

Laboratório Nacional de Energia e Geologia (LNEG), Lisbon, Portugal

ARTICLE INFO

Keywords:
nZEB
BIPV
Multigeneration prototype
Techno-economic analysis

ABSTRACT

The present study explores the contribution and benefits of a renewable energy based multigeneration prototype integrating a luminescent compound parabolic concentrator, a photovoltaic/thermal system and thermal storage using phase change materials. A numerical model was developed for assessing the energy performance of the prototype and the results are presented for three different European locations. A simplified economic analysis was also developed and presented for two different scenarios and the same European locations. The results reveal that the installation of the IDEAS system in Lisbon, with a total estimated yearly use of solar energy of 1215 kWh and an amount of energy sold to the grid of 40.6 kWh, results in savings of 266 € (26 % of energy bill). For the Ferrara location, with a total estimated yearly use of solar energy of 967 kWh and 19.8 kWh of energy sold to the grid of, results on 229 € (16 % of energy bill) of annual savings. In Dublin, with a total estimated yearly use of solar energy of 862 kWh and an amount of energy sold to the grid of 20.5 kWh, results on annual savings of 257 € (14 % of energy bill).

1. Introduction

Buildings are central to the global energy balance, and in Europe, decarbonizing this sector presents a critical challenge. Large-scale deployment of nearly Zero Energy Buildings (nZEBs) is key to achieving this goal. The revised 2024 Energy Performance of Buildings Directive (EPBD) [1] introduces more ambitious targets, aiming to reduce GHG emissions in the building sector by at least 60 % by 2030 (compared to 2015 levels) and to achieve a fully decarbonized, zero-emission building stock by 2050. One of the core requirements of the former directive, EPBD 2010 recast [2] mandates nearly Zero Energy performance, achieved through local alternative energy supply systems that are *cost-efficient* and environmentally sustainable [3,4]. This performance level serves as a milestone towards zero-carbon buildings for new constructions by 2028 and for existing buildings by 2030.

To qualify as an nZEB, a building must incorporate tailored energy-efficient solutions along with renewable energy generation. This requires a focused development of alternative energy sources for the built environment. Solar energy, typically integrated through solar generating systems embedded within opaque sections of the building envelope, is one of the most effective renewable energy solutions for buildings. Façade elements can enhance a building's energy flexibility by optimizing thermal performance to align with the climate and usage patterns, or by adapting dynamically to changing conditions through automated features. Innovative façades with integrated solar energy systems can significantly reduce a building's energy demand, offering a transformative approach to energy-efficient design in the built environment [5].

A sustainable integration of the renewable energy, in order to assure the balance between the architectural aspects, structural and efficiency of the systems, is not always straightforward and consensual, mainly between architects but also engineers. Bot et al. [6] published an extensive review of studies concerning building integrated solar energy systems for façades in the last five years. One of the most used technologies as an integrated system are photovoltaic (PV) modules. The integrated photovoltaic modules in the building envelope are a promising technology that has been widely studied and used due to its multifunctionality. PV systems can even replace conventional construction elements and generate electricity and heat simultaneously, being in this cases called building integrated photovoltaic (BIPV) systems.

Photovoltaic thermal (PVT), a well-known technology and highly investigated in the last 30 years, combine PV with a solar thermal

This article is part of a special issue entitled: ZCBE-1 published in Renewable Energy.

* Corresponding author.
E-mail address: laura.aelenei@lneg.pt (L. Aelenei).

https://doi.org/10.1016/j.renene.2025.123002
Received 2 December 2024; Received in revised form 24 March 2025; Accepted 27 March 2025
Available online 28 March 2025

collector, which transfers the otherwise unused waste heat from the PV module to a heat transfer fluid. Kumar et al. [7] and Herrando et al. [8] developed research reviews regarding conceptual designs of PVT types (according to the integration solutions), evaluation and performance. According to Masood et al. [9], the concentrating PVT may offer benefits in terms of the system optimization, intensifying solar radiation and lowering costs. In the case of BIPV, only about 16 % of the solar energy incident on the PV is converted to electricity, the remaining, being absorbed and transformed into heat [10]. This leads to potential overheating problems for BIPV with an undesirable decrease in the electrical efficiency of the PV cells. To mitigate this problem, a cooling fluid, usually water or air, can circulate behind the module to remove and eventually use the thermal energy from BIPV systems [11]. BIPV/-Thermal systems deliver solar thermal heat at levels similar to conventional solar thermal collectors and generate electricity similar to standard PV modules. Knowing that thermal applications often require higher operational temperatures, whereas the PV module efficiency drops with increasing temperature, a careful architectural design of BIPV/T systems is crucial, and different solutions have been studied to increase the electrical power production from PV modules in addition to the recovery of heat extracted. For example, the evacuation of the accumulated heat through the ventilation of the air gap on the back of PV module, is one way, that may contribute for indoor heating of the adjacent room [11].

In order to increase the PV system efficiency, innovative solutions have been found, especially with the integration of photovoltaic modules in the building façade combined with passive innovative materials, such as Phase Change Materials (PCM) [12–27] or even combined with traditional and natural solutions as water tanks [28]. The type of PV cells also determines the PV module efficiency and consequently the BIPV performance. Single junction photovoltaic (PV) devices exhibit a bottleneck in their efficiency due to incomplete or inefficient harvesting of photons in the low- or high-energy regions of the solar spectrum [29]. In the PV devices, the charge carriers photogeneration only occurs when the energy of solar photons (Eph) is equal or greater than the energy band gap (Eg) of the PV material and all photons with Eph $<$ Eg pass through it and are wasted. Spectral converters exploiting photoluminescence processes have been used to capture low or high energy photons that cannot be used by the PV cell and convert them into photons with useful energy [30]. Luminescent down-shifting (LDS) converters are coatings applied on the PV cell top surface, to absorb the incident radiation complementarily to the PV cell, which is re-emitted at a specific wavelength and then refracted towards the PV cell, allowing to tune the absorption spectral range of the PV device. An ideal material for luminescent down-shifting should possess the following characteristics: (i) broadband absorption, particularly in the region where the spectral response of the solar cell is low; (ii) high absorption coefficient and high luminescence quantum yield (PLQY) so that all incident light results in emission; (iii) high transmittance and narrowband emission, particularly in the region where the device response is high; (iv) large Stokes shift to minimize the self-absorption energy losses due to the spectral overlap between the absorption and emission bands; and (v) long-term stability. Two different architectures have been widely explored to integrate down-shifting converters into PV cells: (1) LDS layer which is a planar design, where the down-shifting material is applied as a luminescent coating on the top surface of the PV cell [31] and (2) a Luminescent Solar Concentrator (LSC) structure, in which the luminescent material is either coated on, or doped within, a transparent waveguide slab, that has PV cell(s) coupled to its edges [32]. In addition to the photoconversion efficiency (PCE) enhancements, it is possible to select LDS materials whose optical absorption is in the UV region of the solar spectrum. In this way, LDS converters could also impact the long-term stability of solar cells by reducing harmful UV absorption in the active layer. Whilst the same role could be fulfilled by a UV filter, the LDS layer has the advantage of not blocking incident UV light, "recycling" it to be used for photocurrent generation [33,34]. Si-based solar cells are currently the most widely used mainstream cell type for solar energy application, as they comprise 85–90 % of the global PV module production. Multicrystalline silicon (mc-Si) solar cells have significantly lower External Quantum Efficiency (EQE) at short wavelength (300 nm–400 nm), due to the low absorption and high reflection caused by the antireflective coating (ARC) between surface–air interfaces, which is mainly optimized for long wavelengths. Although crystalline silicon (c-Si) solar cells show a better performance up to a 400 nm wavelength, there is still a severe decrease in the performance at wavelengths $<$400 nm, thus, the use of LDS layers can be one possible way of enhancing the response at shorter wavelengths. Different luminescent materials such as organic dyes (e.g Lumogen F 570) [35], quantum dots (e.g $CuInS_2$/ZnS and $CH_3NH_3PbBr_3$) [36–39] and europium (III) (Eu) complexes [40] have been employed in LDS layers to enhance efficiency of Si-solar cells.

To assess the PV system integrated performance or even the optimizations, design numerical tools are used, given that experimental studies are most of the time not very easy to set-up and could require additional high investments. Performance assessment methods of the BIPV systems have been addressed by many authors through the use of numerical tools [41–45] or by means of experimental approaches [46].

Some of the numerical tools usually used for modelling solar system integration in buildings and assessing their behaviour are Computational Fluid Dynamics (CFD) simulation software, TRNSYS®, ENERGYPLUS®, MATLAB/SIMULINK®, among others.

Herrando et al. [47] developed and used a modelling methodology to investigate the technoeconomic performance of Solar Combined Cooling, Heating and Power (S-CCHP) systems based on hybrid PVT collectors. A university campus was selected as a case study to demonstrate how the methodology can be used to analyze the suitability and value of these systems when providing space heating, cooling and electricity to the campus buildings. The building energy demands were inputs to a transient system model, which coupled PVT solar collectors via thermal store to commercial absorption chillers. The results showed that a 1.68 MWp S-CCHP system can cover 20.9 %, 55.1 % and 16.3 % of the space-heating, cooling and electrical demands of the Campus, respectively, with roof-space availability being a major limiting factor. Due to the considerably higher investment cost of the S-CCHP system compared to a PV system with the same power, the payback time of the former is significantly higher (16.7 years vs. 6.1 years), being the cost-competitiveness of the solar systems considered very sensitive to the utilities prices.

Braun et al. [48] investigated the potential of a PVT system to heat and cool office buildings in three different climate zones. In this regard, a parametric simulation study was carried out to evaluate system design with different PVT surface areas and storage tank volumes, for two different construction standards. It was shown that with a maximum utilization of PV electricity for heating, ventilation, air conditioning and other electricity demand such as lighting and plug loads, high solar fractions and primary energy savings can be achieved, although the system has not yet been validated under real operation conditions. Nevertheless, the economic feasibility strongly depends on country specific energy prices and energy policy.

Numerical tools are usually used according to the objectives of each study, and with the availability and time necessary for processing. Most of the numerical tools can be used not only for assessing a whole building's performance but also as a specific component. In fact, some of the tools are used for i) detailed analysis of a specific process (heat transfer, flow rate) and strategies (passive/active), ii) designing of the systems and buildings (open studio) or iii) used for optimization purposes [13,23]. A detailed review about the use of the numerical tools used in the design and performance modelling of the BIPV was published in the International Energy Agency Report [42]. The report clearly structured the tools usually used for the design including the management of the integrated PV and corresponding key aspects regarding cost and economics [49–57].

In [50], a solar trigeneration system for an urban single family

dwelling, based on PVT collectors, PV modules and a heat pump unit for Domestic Hot Water (DHW), heating and cooling, was modelled to estimate its thermal and electric yields. The results led to an annual thermal solar fraction of 64 % and an annual electric solar fraction (i.e., the ratio between local PV production and total electric demand) of 103 %, showing the system's positive net energy balance. This work was done for the Portuguese project SOL3 which was a predecessor of project IDEAS.

Within the framework of the European project "IDEAS-Novel building Integration Designs for increased Efficiencies in Advanced climatically tunable renewable energy Systems" [58], an innovative trigeneration prototype was proposed for integration in building façades. The prototype integrates c-Si cells with an LDS layer on the top surface of the PV cell, a compound parabolic concentrator (CPC), a photovoltaic/thermal (PVT) system and thermal storage using phase change materials (PCM). The CPC/PVT/PCM prototype hereinafter referred as "Omega system" is the main component of the general IDEAS integrated system, which apart from this, integrates a heating and cooling system and other building components such as appliances and radiant floor. In the Omega system, the capture of solar radiation is enhanced through the CPC concentration technology and the application of LDS layer in Si PV cell, to increase the production of electricity. With improved solar capture, the temperature of the photovoltaic cells increases, penalizing the PV efficiency. This negative effect is overcome through the installation of heat sinks incorporating PCM that promote cell temperature regulation. The heat released by the PVT can thus be stored and used in domestic hot water (DHW), in a space heating system using radiant floor or used coupled to aerothermal and/or geothermal heat pumps to lower the temperature of the PV. Scientific and Technological Objectives of IDEAS project include: 1) Design of novel LDS layers using high quantum efficiency luminescent dyes and quantum dots (QDs) to increase the capture of direct and diffuse solar radiation, 2) Design of a building integrated compound parabolic concentrator (CPC) for different climatic locations and acceptance angles and 3) Design and optimization of a heat sink utilizing PCM as Thermal Energy Storage (TES), to capture the waste heat in the system to maintain higher system efficiencies and for heat removal from PV.

A numerical model was developed for assessing the energy performance of the prototype in three different European locations and a simplified economic analysis was also developed and presented for the three locations. The novel prototype was upscaled as a building-integrated component, designed not only to generate power but also to provide hot water and space heating within a building. It is expected that the prototype and this preliminary techno-economic analysis contributes to the market advances in developing trigeneration technologies and consequently to energy transition in built environment.

2. Material and methods

This study evaluates the contribution of a renewable energy generation prototype, the core component of the IDEAS multigeneration integrated system, to the energy balance of a typical household.

A transient numerical model was developed and validated using experimental data from prototype testing. This model was then applied to analyze the building's energy balance and assess the prototype's impact. Additionally, a simplified economic analysis of the Omega system was performed to complement the evaluation.

The methodology is detailed in the following subsections, starting with the numerical model description, followed by the input considerations and concluding with the techno-economic analysis approach.

2.1. Numerical model description

The Omega system is a key component of the IDEAS integrated system. To evaluate the performance of the Omega system within the broader IDEAS framework, a 1-D dynamic simulation model was developed using MATLAB/SIMULINK® and SIMSCAPE®. The part of the model related to the Omega prototype was validated with experimental data. While this study primarily focuses on the Omega system performance, the numerical model incorporates the entire IDEAS integrated system. The model consists of three main blocks, each addressing specific tasks:

Input Data Block: Manages the required data, including vertical façade solar irradiance (W/m^2), ambient air temperature (°C), sun height (°), sun azimuth (°), building energy consumption data (electric power for appliances, W), and Domestic Hot Water (DHW) flow rates (dm^3/s at 50 °C) as well as Omega system material characteristics.

IDEAS System calculation model Block: Represents the computational model of the IDEAS integrated system, divided in 3 sub-blocks representing the three main sub-systems of the IDEAS system, one related with the building characteristics, one related with the heating and cooling systems and one related with the PVT composed by the Omega system integrated with a thermal storage system.

Results Block: Generates graphical outputs of performance metrics and other analysis results.

The overall structure of the IDEAS system numerical model is illustrated in Fig. 1. Data simulation and processing occur in three primary sub-systems, responsible for simulating the heating and cooling subsystem, the Omega and thermal storage sub-system, and the building characterization sub-system.

2.2. Input data

2.2.1. Climate data

Hourly data for solar irradiance on a vertical façade and ambient temperature, derived from Typical Meteorological Years for three selected locations, served as inputs. The locations were Lisbon (Portugal), Ferrara (Italy) and Dublin (Ireland) in order to understand how the system worked in different climatic conditions. To compare the climate conditions in the three different locations, average ambient temperature and vertical plane irradiation monthly values are shown in Figs. 2–4. Lisbon is the location with higher values of average yearly vertical plane irradiation, 1281 kWh/m^2, followed by Ferrara, with 1005 kWh/m^2 and Dublin with 845 kWh/m^2. For the average ambient temperature, Lisbon is the one with less variation through the year, with an average yearly value of 16.7 °C. Ferrara has the higher amplitude variation of average ambient temperature, with an average yearly value of 14.4 °C, and Dublin is the coldest location with an average yearly ambient temperature of 9.9 °C.

2.2.2. Household building considerations

The building considered for the study is a simple residential house with an area of 102 m^2 (12 m × 8.5 m) and height of 3 m, 5 windows of 1.2 m^2 (3 south oriented). Typical consumption profiles (DHW, Electricity) for a single-family household with 4 occupants were considered.

Fig. 5 depicts the daily profiles of the household building flow rates of freshwater consumption and DHW consumption (at temperature of 50 °C). The estimated average water consumption was 430 dm^3/day and the average DHW consumption at 50 °C was 115 dm^3/day.

In terms of electrical appliances demand, an estimated yearly total demand of 2650 kWh was considered with an average daily demand of 7.0 kWh on weekdays and 7.9 kWh on weekend days. In Fig. 6 the used daily profile of the electrical demand of appliances on weekdays is presented.

Seasonal variations in day length were not taken into account in the electricity demand due to lighting, because the demand of LED lamps today is negligible in relation to the rest of the household's demand.

2.2.3. Characteristics of the omega components

The Omega system (Fig. 7) was designed to be mounted on vertical façades south oriented and its main characteristics are presented in Table 1. Under standard test conditions (STC), the power of PV modules

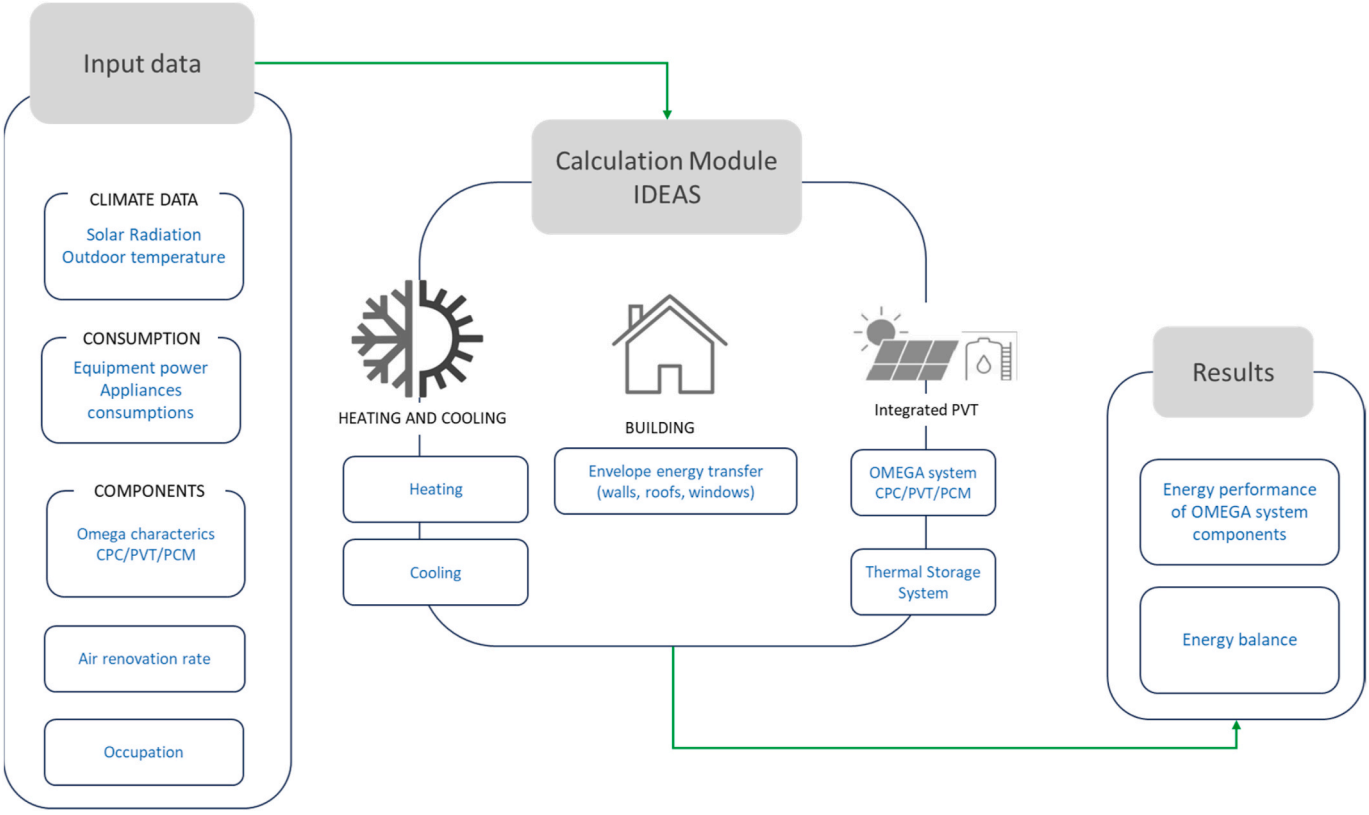

Fig. 1. IDEAS model architecture.

installed in Ferrara without CPC reflectors is near Ppv stc = 113.6 W considering a PV cells conversion area of Acel = 0.5 m^2. The results obtained at Ferrara site between September 2021 and May 2022 were considered to model the Omega system. Based on the measured values, the estimated power of the Omega system at STC conditions was about 140 W with a PV efficiency of 7.3 %.

The characteristics of the PV module of the Omega system are presented in Table 1. The heat released is absorbed by PCM and it is assumed that the thermal absorption of the PV cells is 95 % and this is the amount of energy that reaches the PCM.

The characteristics of the PCM integrated in Omega system are presented in Table 2.

2.2.4. Air renovation rate

For this model an air renovation of 0.50 renovations/h was considered to calculate the amount of thermal power lost or gained by the house, and regarding the activity of each person and their dissipated heat, an average power of 50 W/person was considered, as for the heat generated by the appliances, is assumed that all the energy consumed is converted to heat inside the building.

2.3. IDEAS calculation module

The calculation block of the IDEAS system was divided in three main blocks corresponding with the main IDEAS sub-systems. Each subsystem model is described in the following section.

2.3.1. Integrated PVT: omega and thermal storage systems

In the numerical model, this subsystem is divided into four different blocks: one responsible for the modulation of the CPC optical system, one responsible for the calculations of the photovoltaic conversion, one responsible for the conversion of the Direct Current (DC) power produced by the PV into Alternating Current (AC) power, and finally a block that contains the thermal energy transfer with the PCM. Fig. 8 illustrates the components contained inside the Omega system. A heat sink incorporating PCM was designed and modelled for enhanced heat management. The PCM was installed on the back of the PV cells and its characteristics per c-silicon are shown in Fig. 8.

For the PV cell model, the power output, P_{pv}, was calculated as a function of incident irradiance at the cells, $G_{i\ cel}$, the cells temperature, T_{cel}, and Standard Test Conditions (STC) for the PV power, temperature and irradiance, $P_{pv\ stc}$, T_{stc} of 25 °C and G_{stc} of 1000 W/m^2.

$$P_{pv}(G_{i\ cel}, T_{cel}) = P_{pv\ stc}.\frac{G_{i\ cel}}{G_{stc}}.[1 + \gamma.(T_{cel} - T_{stc})] \quad (1)$$

Where γ is the cells coefficient of variation of maximum power with temperature.

Equation (2) shows how some of the incident solar power in the external area of the CPC/PVT module, $G_{i\ mod}.A_{mod}$ is lost due to the optical losses in the CPC design and reflectivity of mirrors, CPC_{losses}, leading to the effective solar power at the cells surface, $G_{i\ cel}.\ A_{cel}$,

$$G_{i\ cel}.A_{cel} = G_{i\ mod}.A_{mod}.(1 - CPC_{losses}) \quad (2)$$

A CPC optical losses factor function of the sun height, h_{sun}, and azimuth, z, was considered. The losses were estimated for the Ferrara site from the prototype electrical power data, P_{pv}, at different sun heights and azimuths, considering the STC temperature. The five coefficients of the sine of the solar height angle and solar azimuth angle polynomial equations, $P(z)$ and $P(\sin(h_{sun}))$ used to model the optical losses associated with the CPC geometry are shown in Tables 3 and 4.

The available solar power for conversion at the cells is given by the product of CPC losses, CPC_{losses}, irradiance, G_i, and the total cell area, $A_{cel\ tot}$, and the CPC loss factor is calculated by Equation (3).

$$CPC_{losses} = \mathrm{P}(z).\mathrm{P}(h_{sun}) \quad (3)$$

Considering the data results obtained at Ferrara site with the Omega

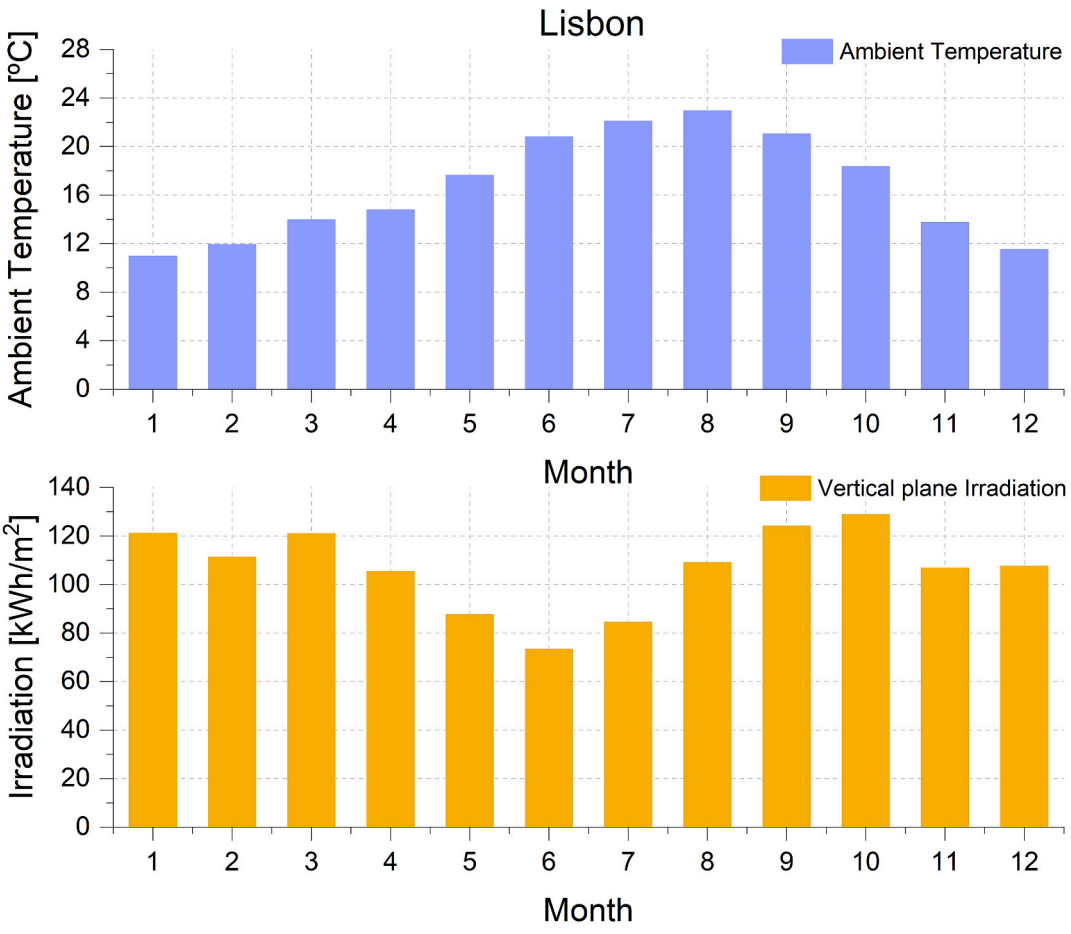

Fig. 2. Average monthly ambient temperature and south facing vertical plane irradiation at Lisbon.

Prototype, a thermal loss at the cell's front of 10 $Wm^{-2}K^{-1}$ and a matching factor between the connected cells of 0.882 are used.

The PV cell's efficiency at a given irradiance and temperature, η_{pv}, is calculated by Equation (4), where η_{stc} is the cell's STC efficiency. A simplified model was used considering T_{cel} (t) to be equal to the temperature of the PCM behind the back of the CPC/PVT module.

$$\eta_{pv}(G_{i\,cel}, T_{cel}) = \eta_{stc}.F_m.[1 + \gamma.(T_{cel} - T_{stc})] \quad 4$$

Considering the results obtained at Ferrara site the equation includes the matching factor losses, between the connected cells, F_m, with a typical value of 0.90–0.95 at conventional PV modules. Mismatch losses are caused by the interconnection of solar cells or modules which do not have identical properties or which experience different conditions from one to another. Mismatch losses are a problem in PV cells, modules and arrays, since the output of the entire PV device is determined by the solar cell with the lowest output, because the cells are connected in series to increase the output voltage.

The thermal behavior of PV modules' cells strongly influence its electrical performance and is determined by an energy balance between ambient temperature and the heating of the cells due to incident irradiance. Adopting Faiman's formula [59], where T_{cel} and T_{amb} are the PV cells and ambient temperatures, G_{i} is the incident solar irradiance, U is the cell's global thermal loss coefficient, and W_{s} is the wind speed, the cell temperature can be obtained by Equations (5)–(7).

$$U.(T_{cel} - T_{amb}) = \alpha.(1 - \eta_{pv}).G_{i\,cel} \quad 5$$

α is the thermal irradiance absorption coefficient and η_{pv} is the PV efficiency conversion.

$$U = U_0 + U_1.W_s \quad 6$$

U_0 and U_1 are the thermal coefficients describing the effect of the cooling by convection and the wind, respectively [60].

$$T_{cel} = T_{amb} + \frac{\alpha.(1 - \eta_{pv}).G_i}{U_0 + U_1.W_s} \quad 7$$

For the prototype, a global thermal loss coefficient of 0.5 $Wm^{-2}K^{-1}$, proportional to the cell's area is used, considering a fully insulated backside, low infrared radiative losses and low wind losses.

The PVT produces DC power, in order to connect it to the AC electrical grid an inverter is needed. The inverter output power, P_{AC}, is a function of its efficiency curve and of the PV input power, P_{DC}. The power produced by the PV module is a function of its temperature, operating voltage and incident solar irradiance. The inverter is equipped with a Maximum Power Point Tracking (MPPT) device that adjusts the operating voltage so that the modules operate at their maximum power point at all times. For each set of modules, one inverter with a typical conversion efficiency curve, η_{inv} (P_{DC}/P_{nom}), which is a function of the normalized input power defined as the ratio between the input power, P_{DC}, and the nominal power of the inverter, P_{nom}, is considered. The modelled inverter efficiency curve is depicted in Fig. 9.

Fig. 10 shows the input parameters used for the Omega system.

The subsystem responsible for modeling the thermal energy transfer with the phase change materials has a mask for parameter input that is shown in Fig. 11.

This model is implemented with 3 subsystems, shown in Fig. 12. One that models and calculates the temperature change of the PCM according to the gains and losses on the CPC/PVT/PCM prototypes, one that calculates the PCM cooling resulting from thermal losses and heat dissipation and another that controls the circulation of the fluid and evaluates if the PCM temperature is enough to produce an energy gain

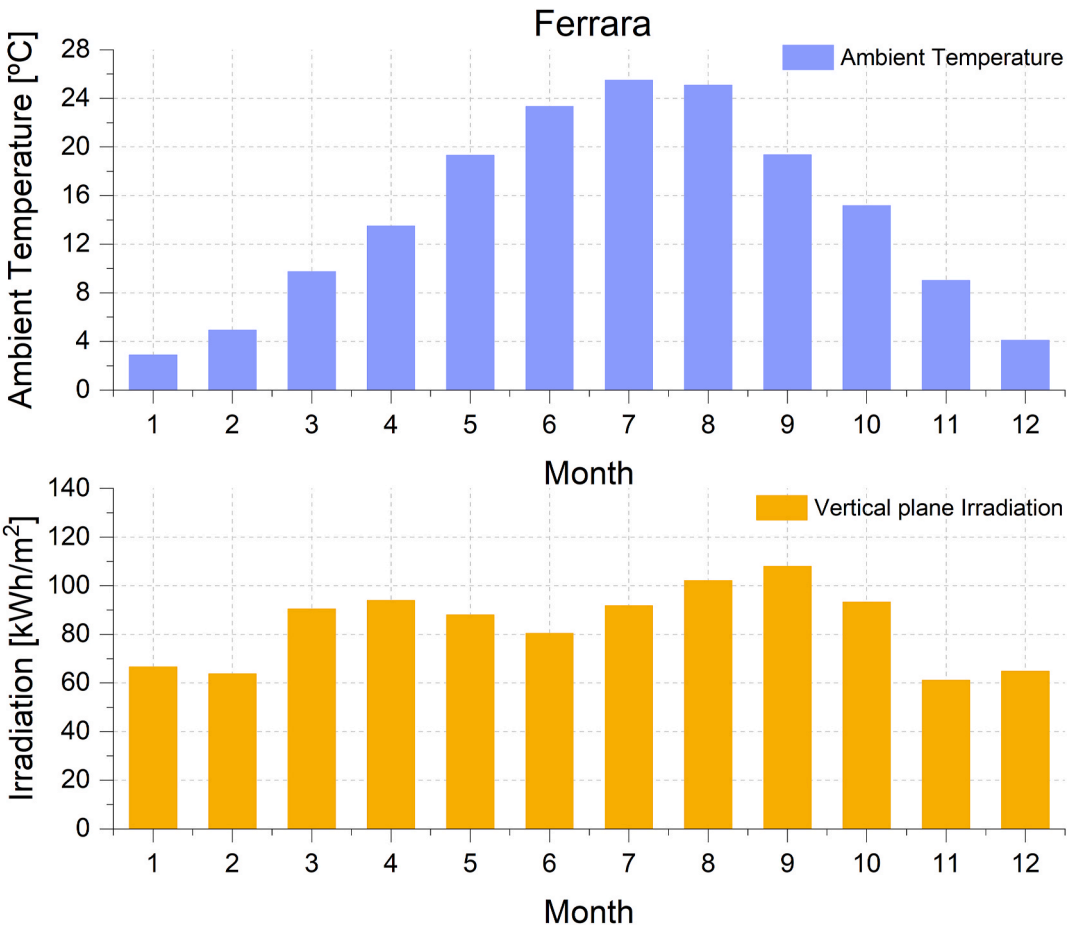

Fig. 3. Average monthly ambient temperature and south facing vertical plane irradiation at Ferrara.

inside the thermal energy system. Only the solar power that has reached the solar cells and has not been converted into electrical energy is available for thermal conversion The thermal gains of the PCM system are all due to the thermal energy that is available at the back of the solar cells. It is assumed that the thermal absorption of the PV cells is 90 % and that this energy reaches the PCM.

The cells/PCM cooling subsystem contains tree different sinks of energy, Fig. 13. The first one, is the heat removed by the fluid that circulates inside the PVT/PCM and goes back to the Thermal Energy Storage (TES) tank to heat the water inside it. The second one, is the power loss to the ambient air. And the third is the power dissipated if the maximum storage tank temperature is reached.

In the model subsystem that calculates the energy removed from the PVT/PCM by the fluid flow rate, a control mechanism is implemented to make sure that two conditions are met before the circuit is activated (Fig. 14). If the PCM temperature is 5 °C higher than the bottom tank layer temperature, the circuit will be activated, but only if the PCM temperature is also higher than the mains water temperature[1].

The circulation works while the PCM temperature is 2 °C higher than the bottom tank temperature and higher than the mains water temperature. The system remains in standby and waits for the solar radiation to heat up the solar cells until the temperature is high enough to activate the circulation again. The subsystem control scheme is shown in Fig. 14.

In the PCM there is a stateflow subsystem that controls at which phase the PCM is in, solid phase, molten mass, or liquid phase, Fig. 15.

In this subsystem's mask, it is possible to change the PCM physical properties to any other values, Fig. 16, allowing the full customization of the PCM material and the amount of mass used on each CPC/PVT/PCM prototype module.

The TES is modelled in the PV&Thermal subsystem. The numerical model of the storage system is designed to calculate the temperature at different layers inside the tank, resulting from the different flow rates at external connected circuits (Fig. 17). Several parameters characterizing the TES can be changed, including the capacity, the tank height, the thermal coefficients losses at top, side and bottom, if DHW is used, the output temperature for DHW, the initial temperatures of the three tank layers and the calculation method for the mains water temperature.

To represent the heat transfer between layers, an approach based on the physical principles of conservation of mass and energy of independent flow rates was implemented. In practice, each of these flow rates are associated with mass and energy flow. It is this mass energy flow that is taken in consideration, since it allows to calculate the average temperature of each layer.

- $\dot{m}_{pvt}$ the flow rate that comes out from bottom layer, at the same temperature of that layer and goes in top layer at the output temperature of the PVT/PCM modules
- $\dot{m}_{dhw}$ the internal flow rate resulting from the DHW consumption
- $\dot{m}_{rfh}$ the flow rate at middle layer that goes out at the temperature of this layer and returns at the temperature of the radiant floor

The temperature of each layer is calculated through an energy balance, Figs. 18 and 19.

It is admitted that the storage tank has a cylindrical shape and that the average heat loss coefficient at the tank bottom surface is equal to

[1] In order to avoid circulation activation during the night when there is DHW consumption and, at the same time, the incoming mains water is warmer than the PCM, which would result in heating the PCM.

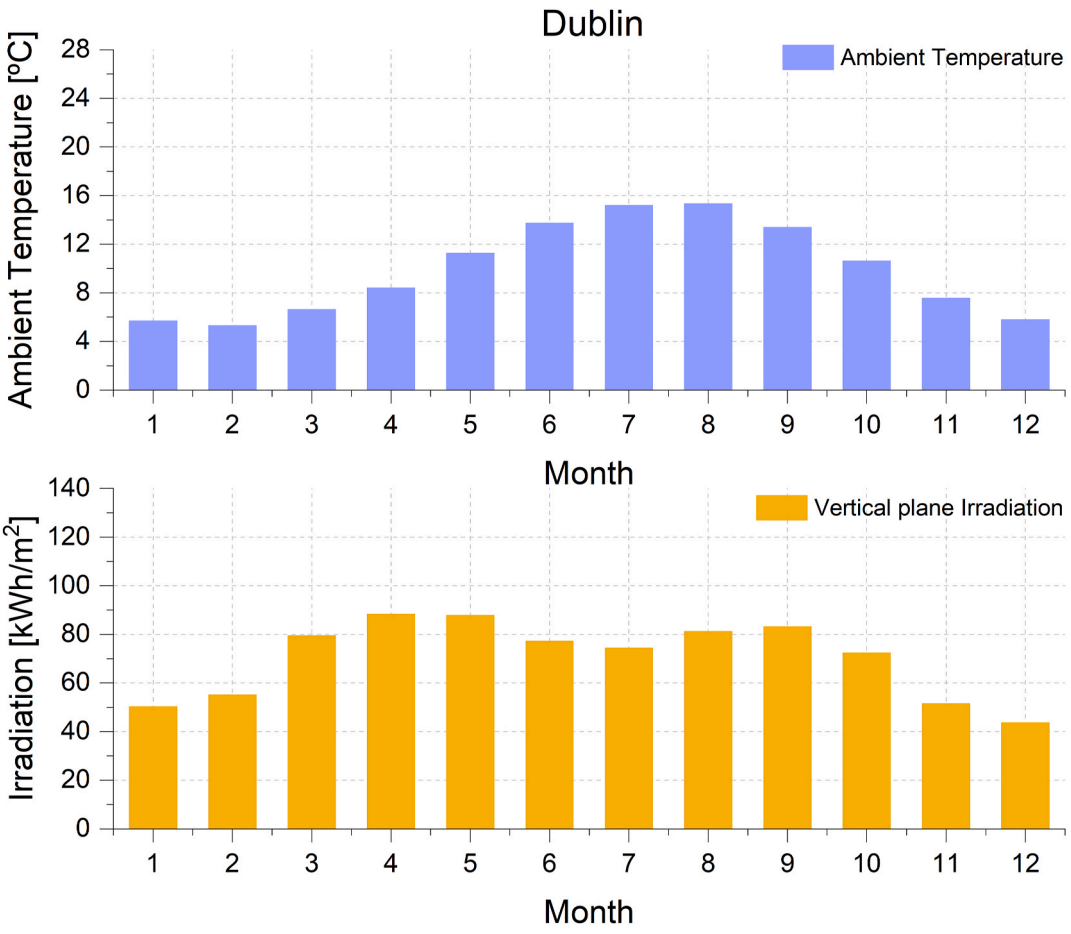

Fig. 4. Average monthly ambient temperature and south facing vertical plane irradiation at Dublin.

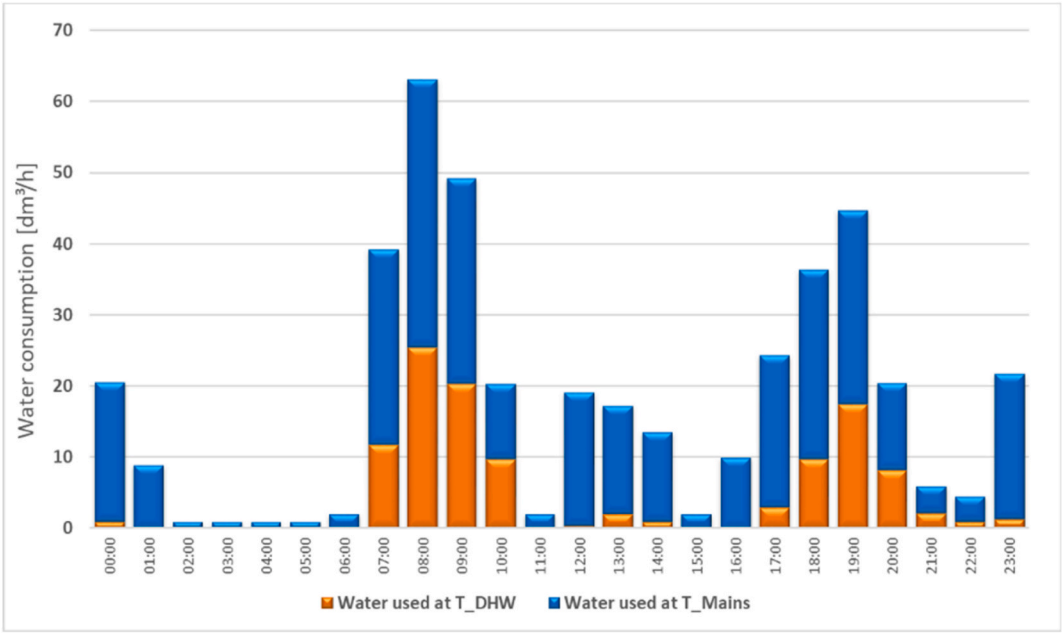

Fig. 5. Household flow rates of water and DHW demands at 50 °C.

3.06 $Wm^{-2}K^{-1}$, while for middle layer it is 0.71 $Wm^{-2}K^{-1}$ and at the top layer it is 0.71 $Wm^{-2}K^{-1}$, Cruickshank et al. [61].

In order to satisfy the consumption of DHW it is considered that the electrical backup system only works if necessary. The DHW is extracted from the thermal storage tank top layer and if the temperature is lower than the set consumption temperature (50 °C) the water is heated to this

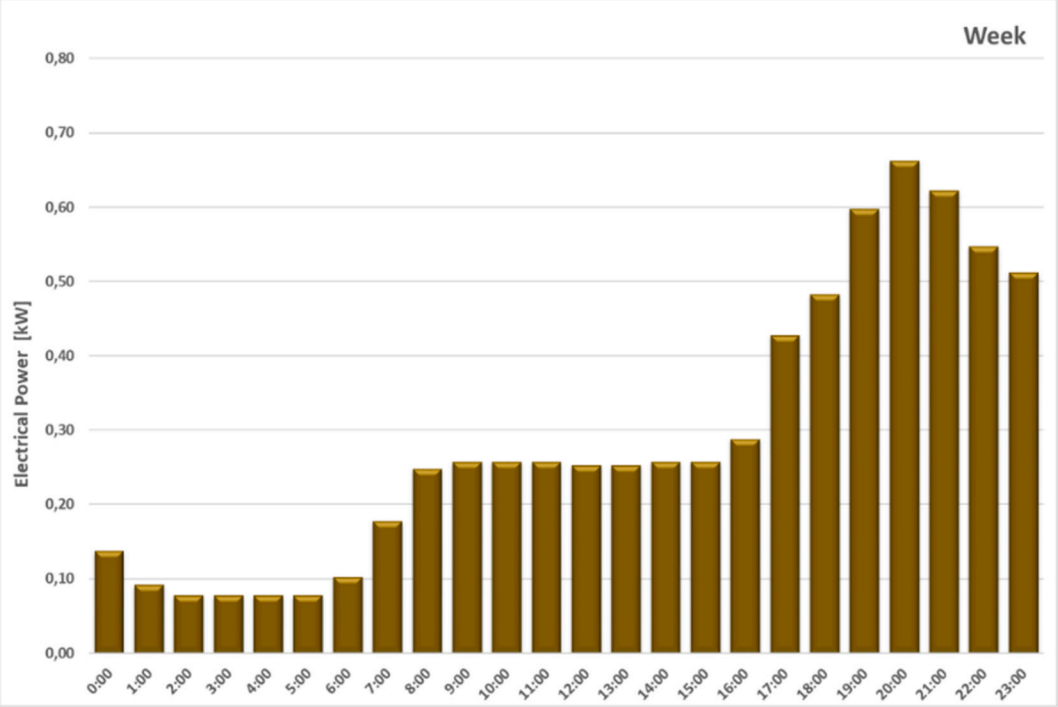

Fig. 6. Daily profile of the electrical demand of appliances on weekdays.

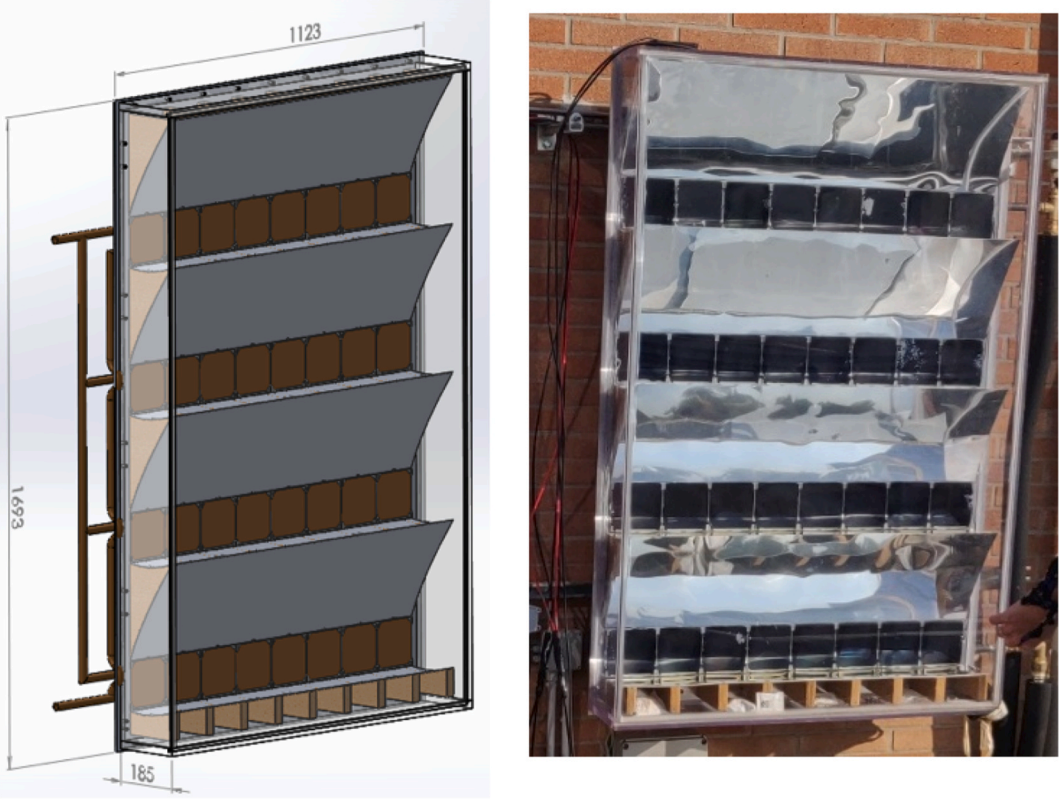

Fig. 7. Omega System installed in Ferrara.

temperature, so that only the consumed water is heated. On the other hand, if the water temperature from the tank is higher than the set temperature for consumption, the extracted water flow rate is adjusted so that when mixed with mains water it guarantees the DHW flow rate and temperature for consumption.

The seasonal variation in the mains water temperature for the different cities was taken into account. It was estimated as a moving average of the ambient temperature with a delay (average of the last 30 days hourly values).

Table 1
Omega-PV characteristics.

Considered parameters	Values
Exterior dimensions	1693 mm x 1123 mm
Total surface [A_{mod}]	1.90 m^2
Estimated STC power [P_{mpp}]	140 W
Number and type of cells	32 monocrystalline cells
Cells area	0.50 m^2
Estimated Module PV Efficiency	7.3 %
Estimated Temperature coeff. of P_{mpp} [γ]	−0.40 %/K
Estimated thermal loss coefficient	10 W/m^2.K
Estimated Prototype Cost	1462 €

Table 2
Omega-PCM characteristics per c-Si PV module.

Considered parameters	Corresponding values
Mass	12 kg
Specific Heat at Solid Phase	2250 J/kg K m^2
Specific Heat at Liquid Phase	2250 J/kg K m^2
Number and type of cells	32 monocrystalline cells
Melting Temperature	36 °C
Latent Heat of Fusion	260 000 J/kg
Initial temperature of Solid Phase	15 °C

2.3.2. *Heating & cooling subsystem*

A Heat Pump (HP) controls the temperature inside the building environment by exchanging heat with the outside. There are 3 essential components to the HP: the outdoor unit (evaporator), the indoor unit (condenser) and the refrigerant that transfers the heat as it circulates between the outdoor and indoor units. The HP can heat the building in a cycle where the evaporator extracts energy from a renewable source (air, water, geothermal or solar) by forcing the liquid to transform into a gas. The compressor compresses the gas, which raises its temperature. The condenser exchanges the heat from the gas to the heating system, and the gas returns to a liquid state. The expansion valve lowers the pressure of the refrigerant, which triggers evaporation, and the cycle begins all over again. Reversing the cycle process, the HP can cool the building. Air-to-water low temperature HPs are considered an optimal choice for new homes or buildings, when combined with underfloor heating or low temperature radiators, because they require less energy for heating.

The HP subsystem is mainly responsible for adjusting the house temperature according to the Heating and Cooling demand of the building.

Moreover, it also allows to adjust the temperature inside the house to the comfort zone predefined by the user. Depending on the country and city where the IDEAS project is implemented, different comfort temperatures are used to make this decision. Fig. 20 shows this susbsystem's mask where the set point parameters can be defined.

The mask of the HP allows some important parameters to be established and changed, namely:

- Turning the HP ON or OFF
- The temperature set point to which the air is heated up or cooled down (restricted to boundaries established by the model)

Table 3
Optical CPC losses - Coefficients of the polynomial equation of the sine of the solar height angle h_{sun}.

$\sin(h_{sun})^4$	$\sin(h_{sun})^3$	$\sin(h_{sun})^2$	$\sin(h_{sun})$	1
15,505652	−31,279978	21,799339	−6,335270	1,434036

Table 4
Optical CPC losses - Coefficients of the polynomial equation of the solar azimuth angle z.

z^4	z^3	z^2	z	1
−3,0806E-08	−2,4239E-06	1,5645E-04	2,8065E-03	−1,4021E-02

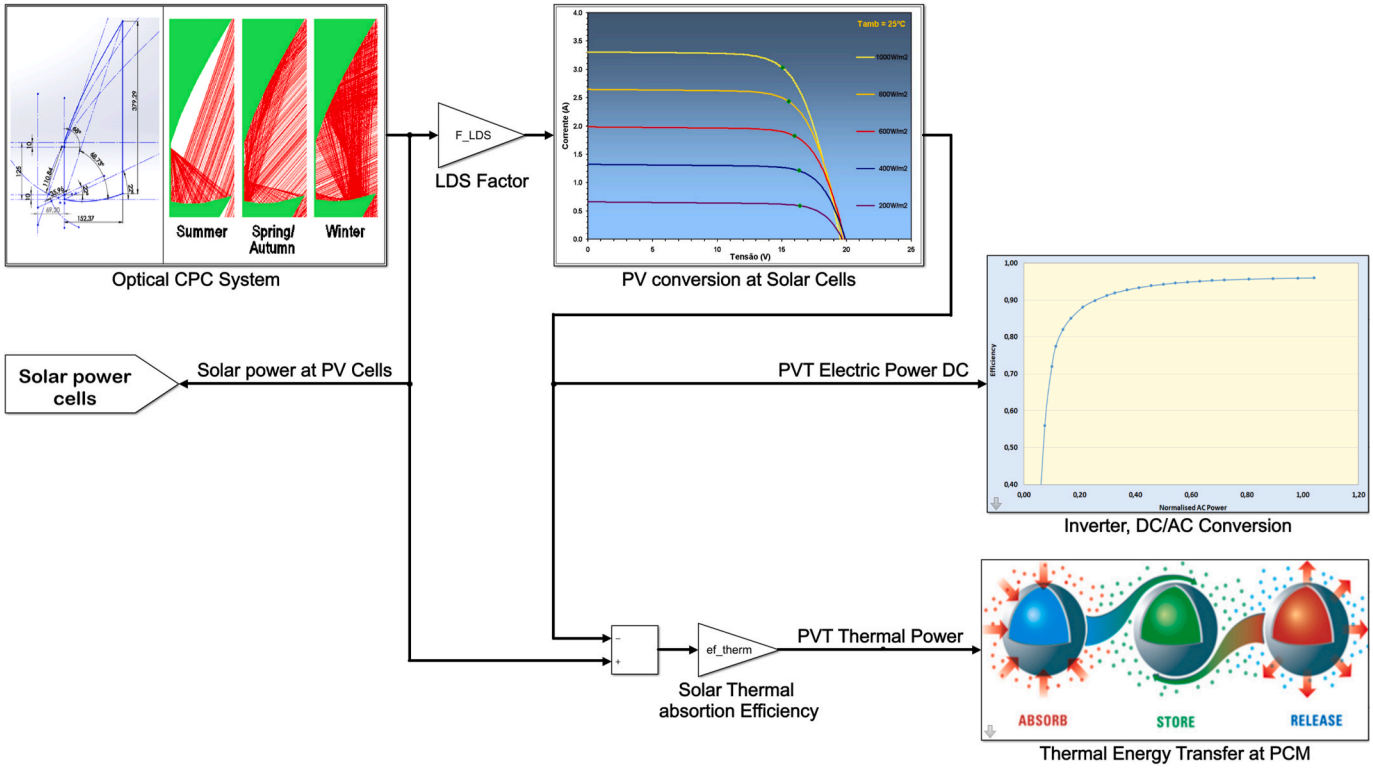

Fig. 8. Omega model structure-electric and thermal parts.

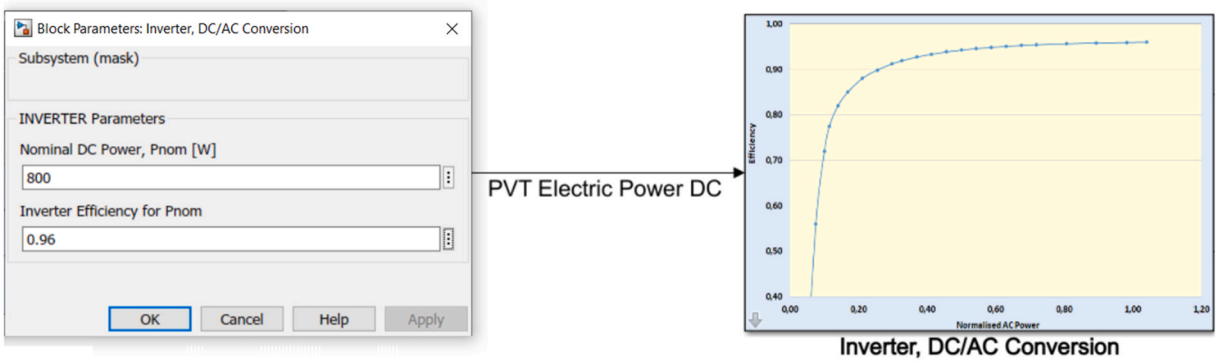

Fig. 9. Inverter parameters and efficiency curve.

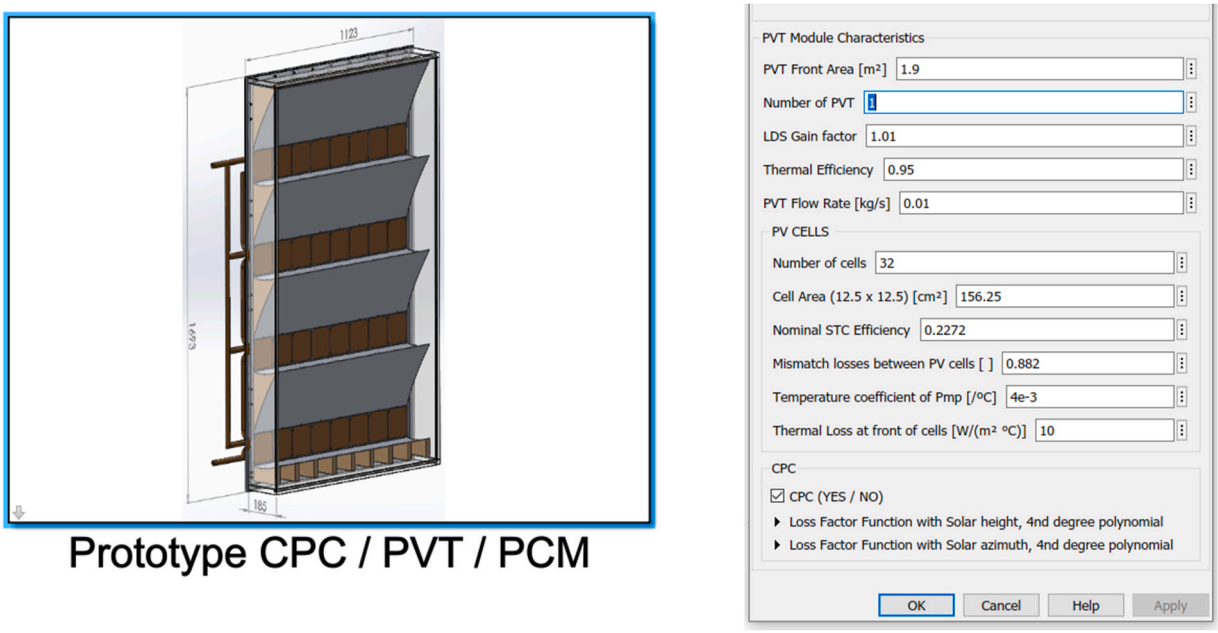

Fig. 10. Omega system parameters.

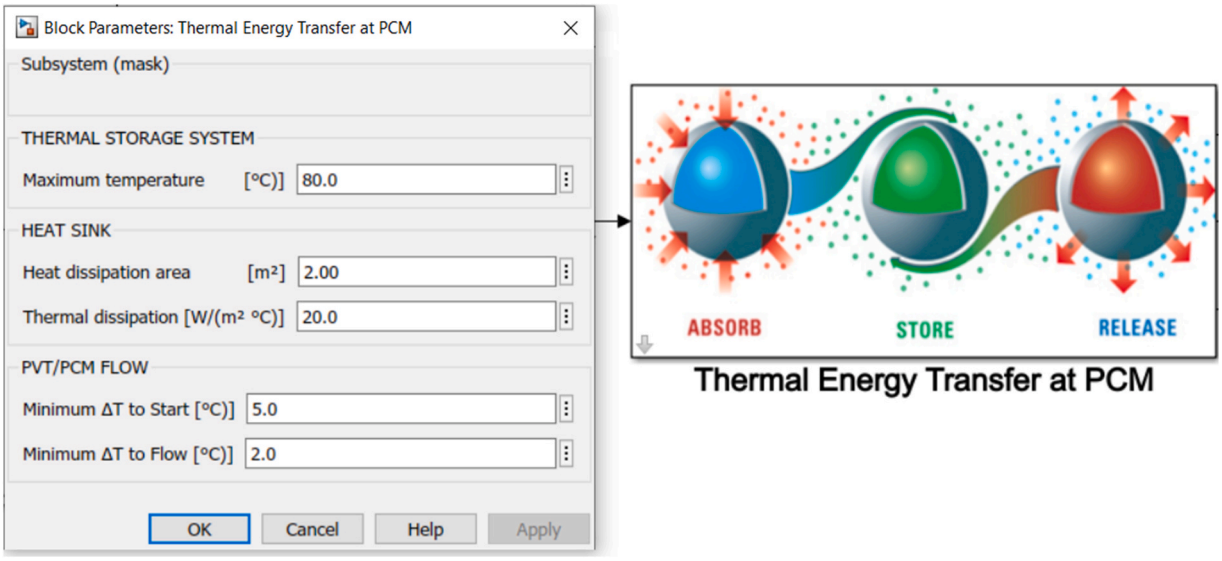

Fig. 11. Thermal energy transfer to PCM mask with the dissipation parameters.

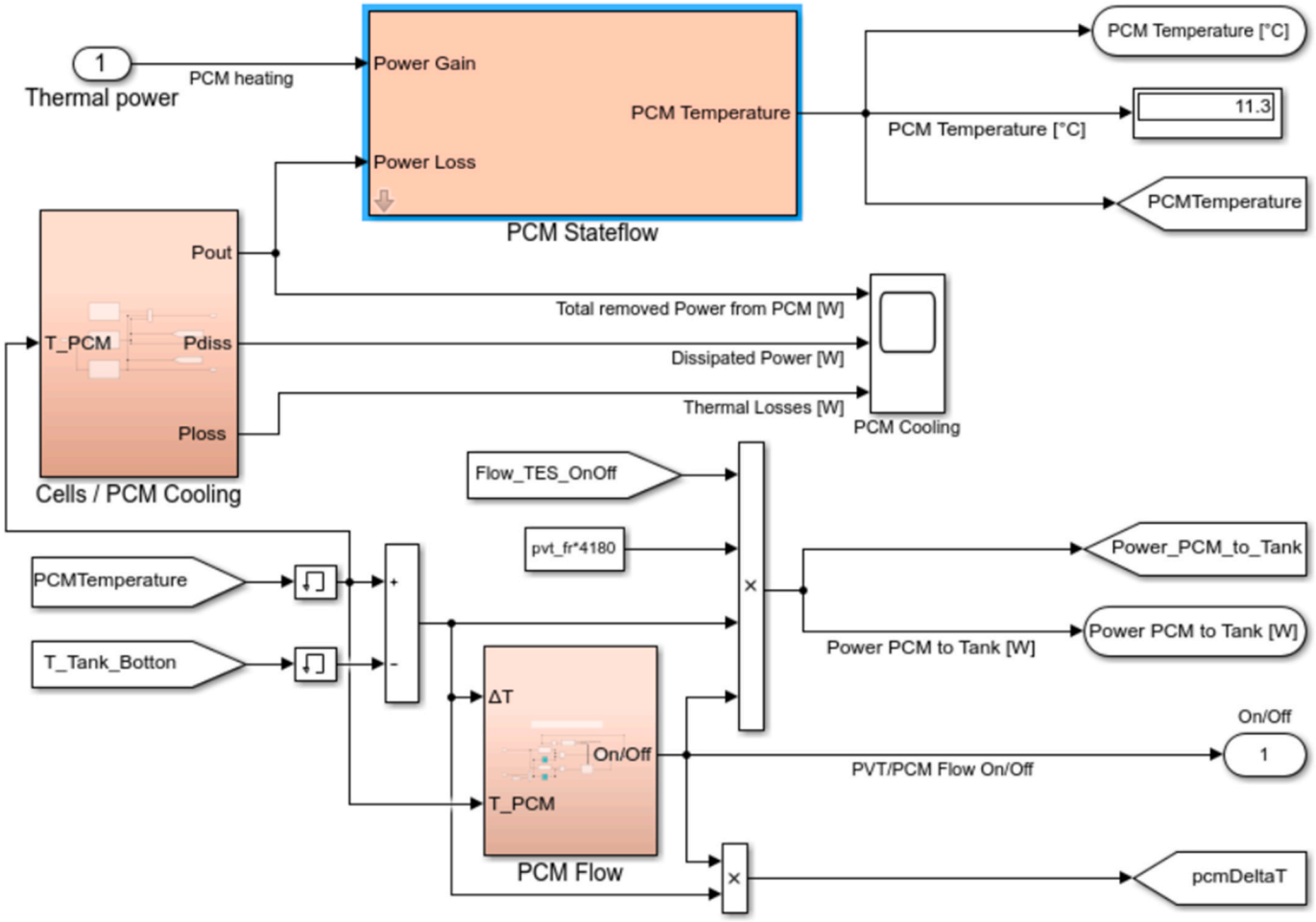

Fig. 12. Pcm System.

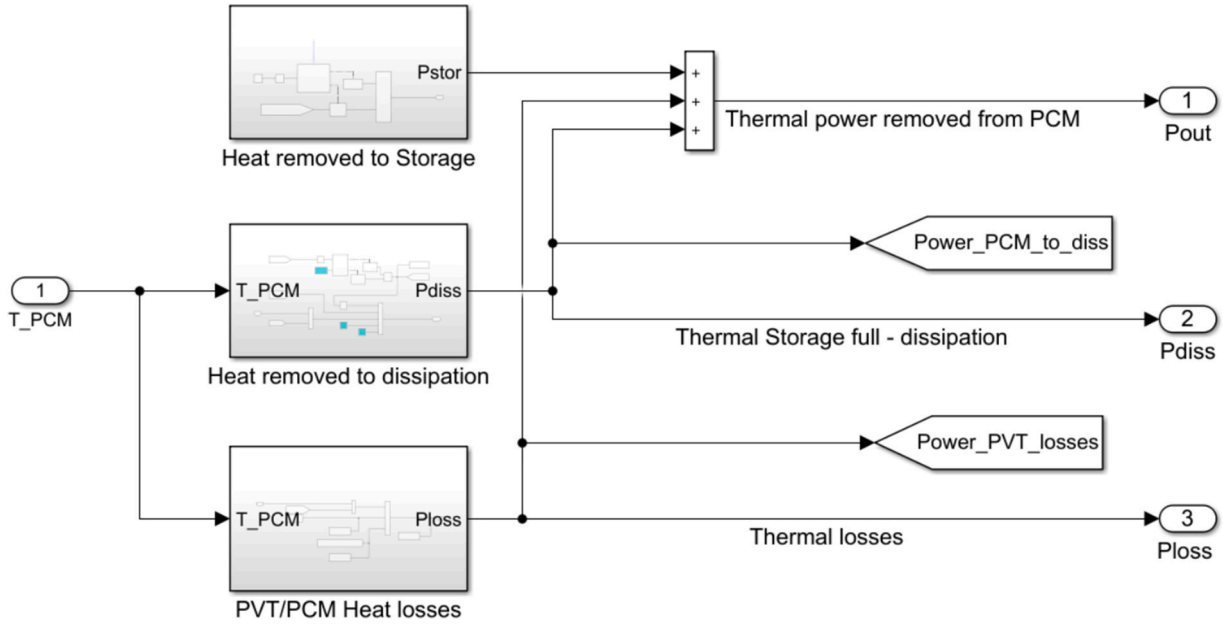

Fig. 13. Cells/PCM cooling system.

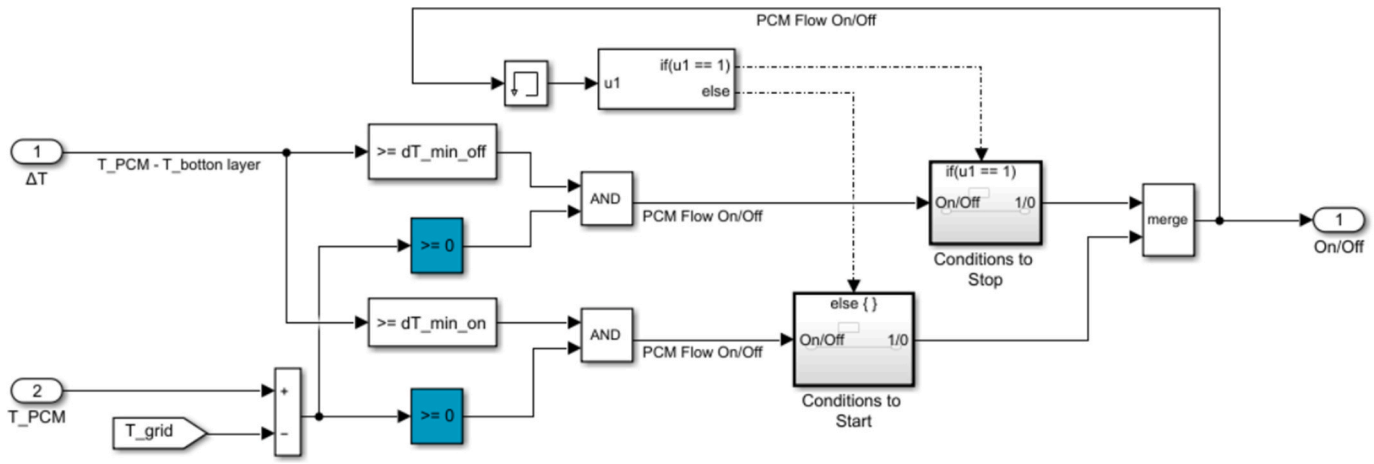

Fig. 14. PCM system flow in the PCM On/Off.

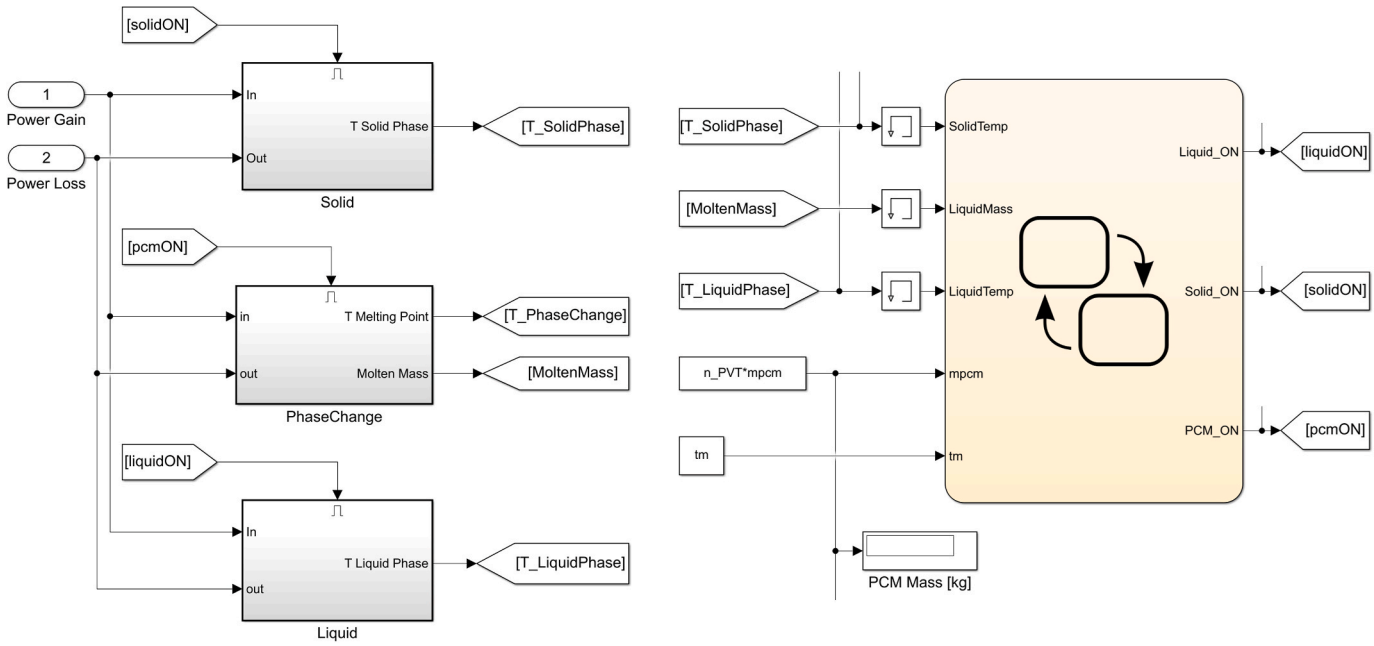

Fig. 15. PCM system interconnection with Stateflow.

- The mass flow rate of the air coming out of the HP and it's specific heat
- Choosing if the model to operates with the IDEAS performances, or with conventional performances
- Defining the values for The Seasonal Energy Efficiency Ratio (SEER)
- Defining the values for The Seasonal Coefficient of Performance (SCOP)
- Defining the values for The Improved Seasonal Energy Efficiency Ratio (I-SEER)
- Defining the values for The Improved Seasonal Coefficient of Performance (I-SCOP)

The improved values are associated with the IDEAS facilities usage. This option will allow the measurement in the Management subsystem of the cost reductions achieved by using Ground Heat Exchangers together with Air Heat Exchangers. These values can be modified according to the results from the experimental data sites of the project. The Standard values were based on a market analysis of HPs from different brands.

Inside the HP there are two subsystems responsible for the operating modes, the Heating control system, and the Cooling control system that are shown in Fig. 21. Both implement Equation (8) that will add or remove heat from the building depending on the indoor temperature.

$$Q_{in} = \dot{m}_{air}.c_{p\ air}.\Delta T \quad (8)$$

Where $\dot{m}_{air}$ is the mass flow rate of air entering the building, $c_{p\ air}$ is the specific heat of air and ΔT is the difference in temperatures between the temperature of the air entering the building and the indoor air temperature. If the building indoor temperature rises, ΔT will be negative, outputting a negative value, wich means that heat should be removed from the inside to the outside.

Fig. 22 depicts the mechanism used to decide which coeficients of performance will be used by the program. The variable that decides if the IDEAS technologies are ON or OFF is called "IDEAS_ON" and can be activated or deactivated at the mask presented at Fig. 20.

The Heat Pump (HP) subsystem is mainly responsible for adjusting the house indoor temperature according to the building demand for heating and cooling and allows to adjust the temperature inside the building to the comfort zone predefined by the user. The same comfort

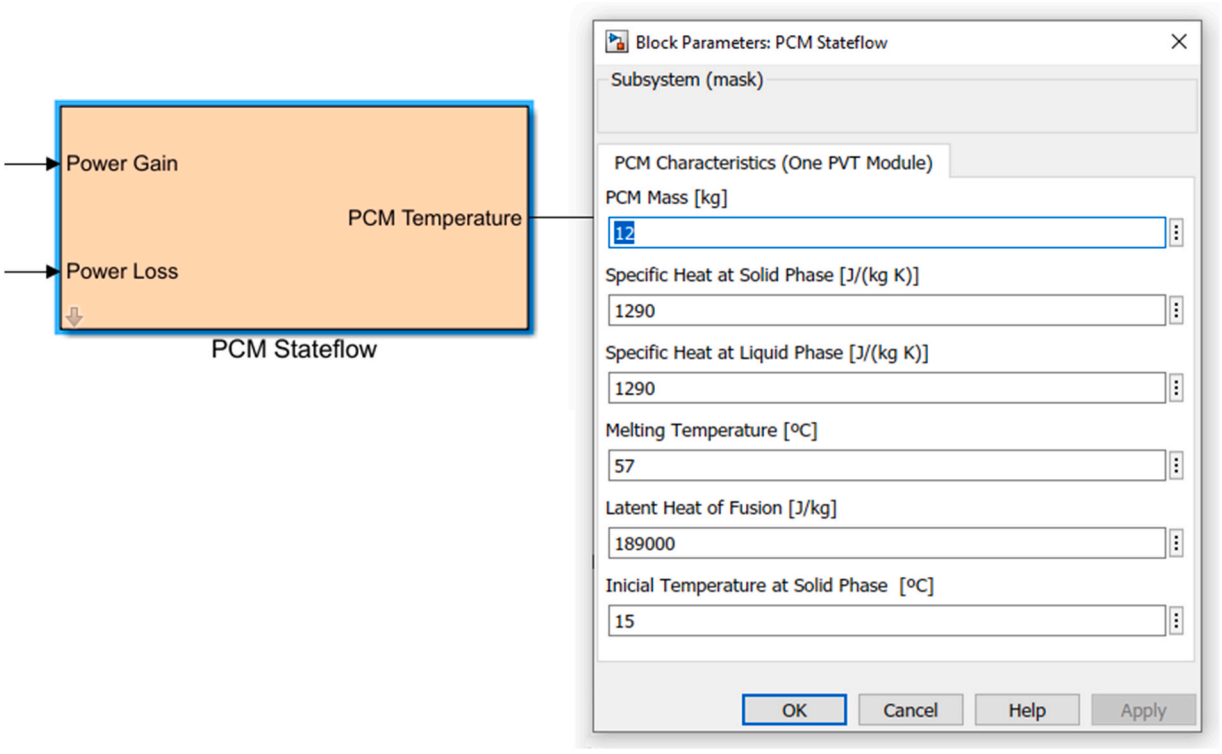

Fig. 16. PCM subsystem mask - example of PCM parameters (DHW use).

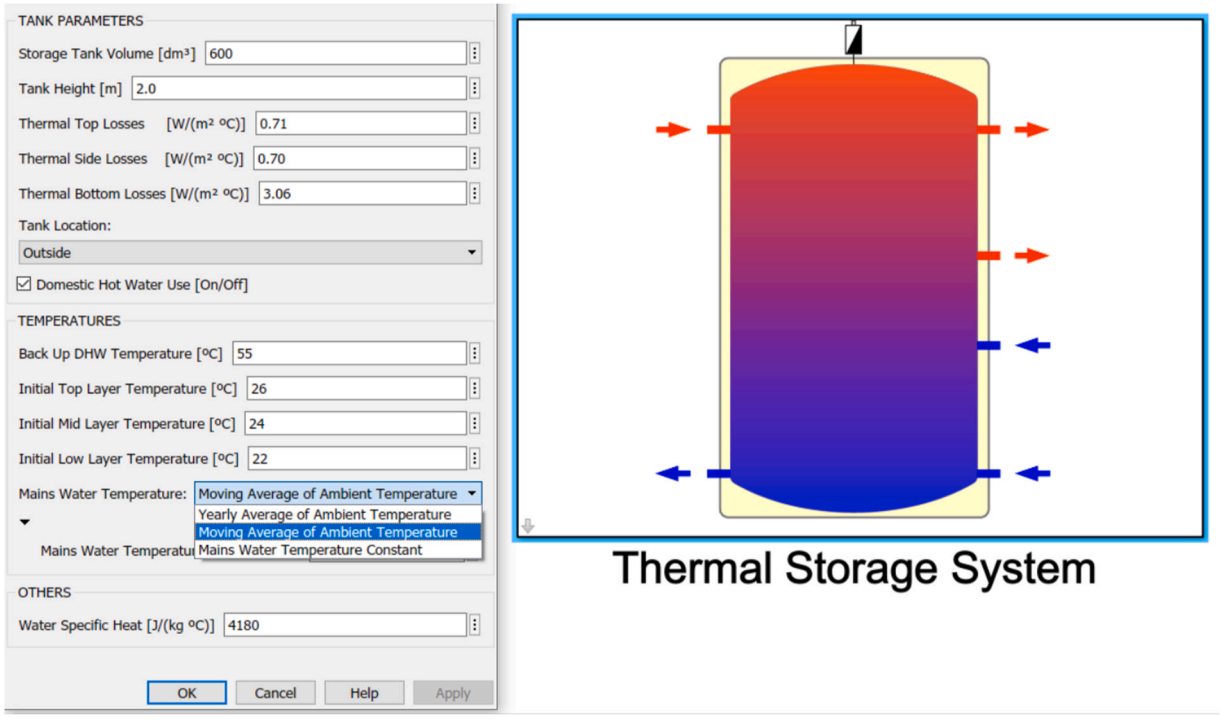

Fig. 17. Thermal storage system input parameters.

temperature set points were considered for the three locations (Lisbon, Ferrara, Dublin), for the heating period, between 18 °C and 20 °C, and for the cooling period between, 23 °C and 26 °C. In order to calculate the eletrical consumption due to the comfort needs, it was considered that the HP system operates at heating with a Seasonal Energy Efficiency Ratio (SEER) of 4.53, and at cooling with a Seasonal Coefficient of Performance (SCOP) of 2.55. These improved values are associated with the IDEAS usage and were modified according to the results from the experimental data from the Ferrara site.

2.3.3. Building subsystem model

This subsystem aims to model a typical standard house or building to

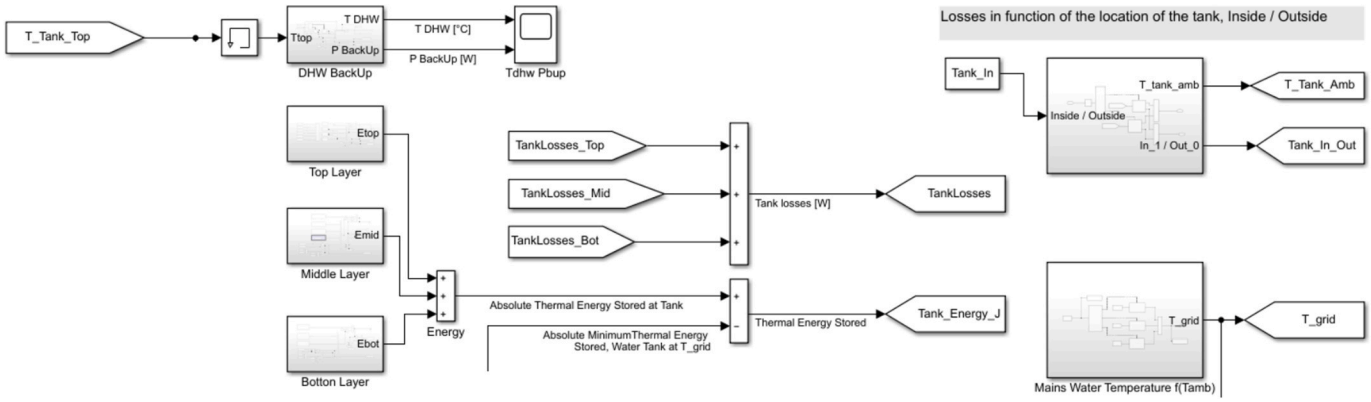

Fig. 18. Thermal storage subsystem model.

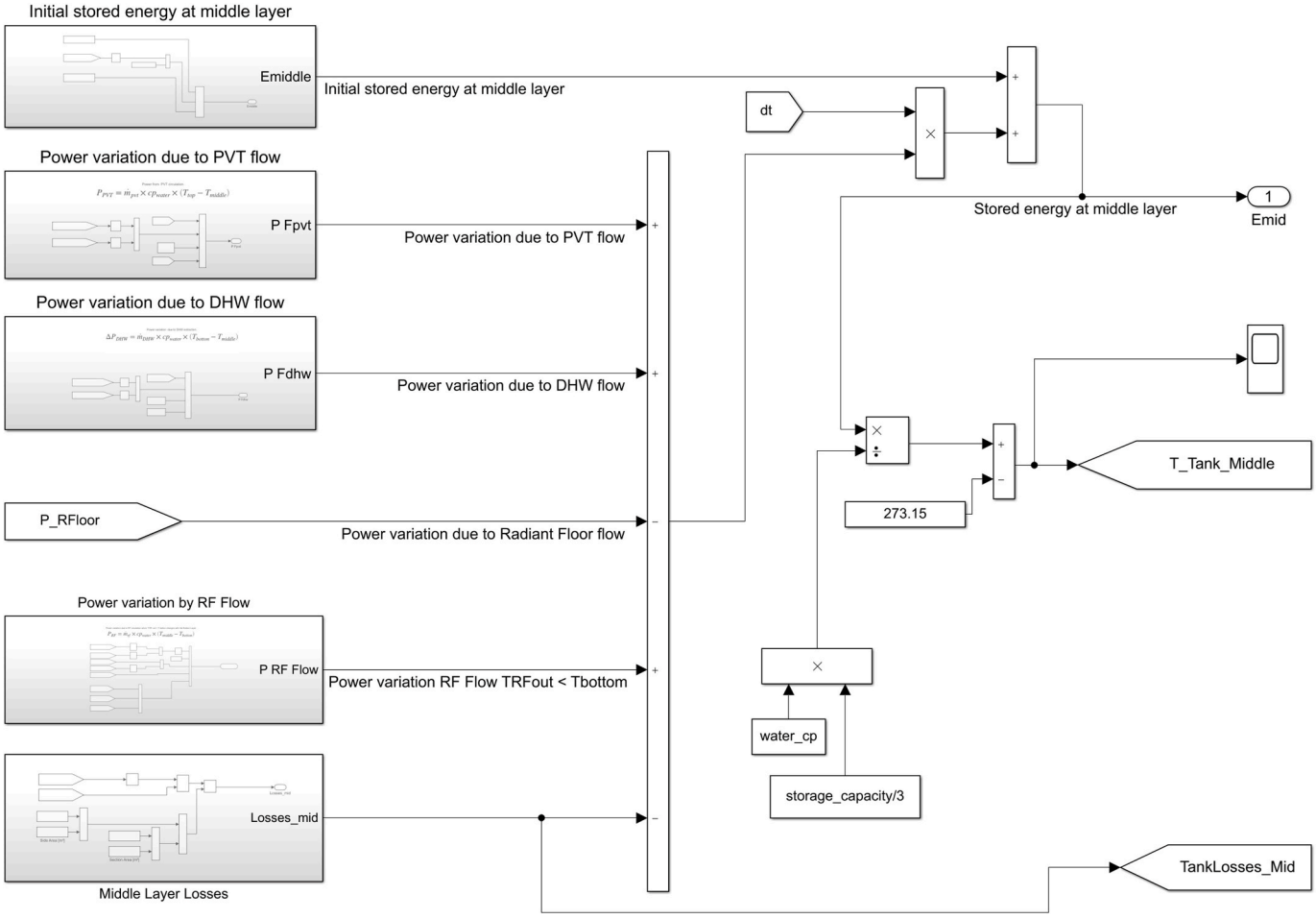

Fig. 19. TES example of Balance of energy at Middle layer block.

estimate how each IDEAS concept will influence energy consumption. The building subsystem model can be observed in Fig. 23 and considers that the building exchanges heat with the environment through its walls and windows. Each component simulates a combination of a thermal convection, thermal conduction, and thermal mass.

This subsystem calculates the indoor temperature as a function of the ambient temperature. It was assumed that the six Omega systems with a total area of 11.4 m^2 were integrated on the building's south façade. In addition to the energy exchanges with the environment, the Building subsystem also calculates the heat transfer coefficient of the walls, windows and the overall coefficient of the building. These values allow the user to make a direct comparison between the energy performance of the building that is being modelled and other buildings, Table 5.

The thermal subsystems in the buildings are modelled based on the concept of thermal equivalent circuit. If a one-dimensional heat transfer with no internal energy generation and with constant properties is assumed, it is possible to create an analogue between the diffusion of heat and electrical charge. Just as an electrical resistance is associated with the conduction of electricity, a thermal resistance, $R_{thermal}$, may be associated with the conduction of heat. Defining thermal resistance as the ratio of a driving potential, $\Delta T=T_1-T_2$, (temperature difference between both sides of the wall) to the corresponding heat transfer rate,

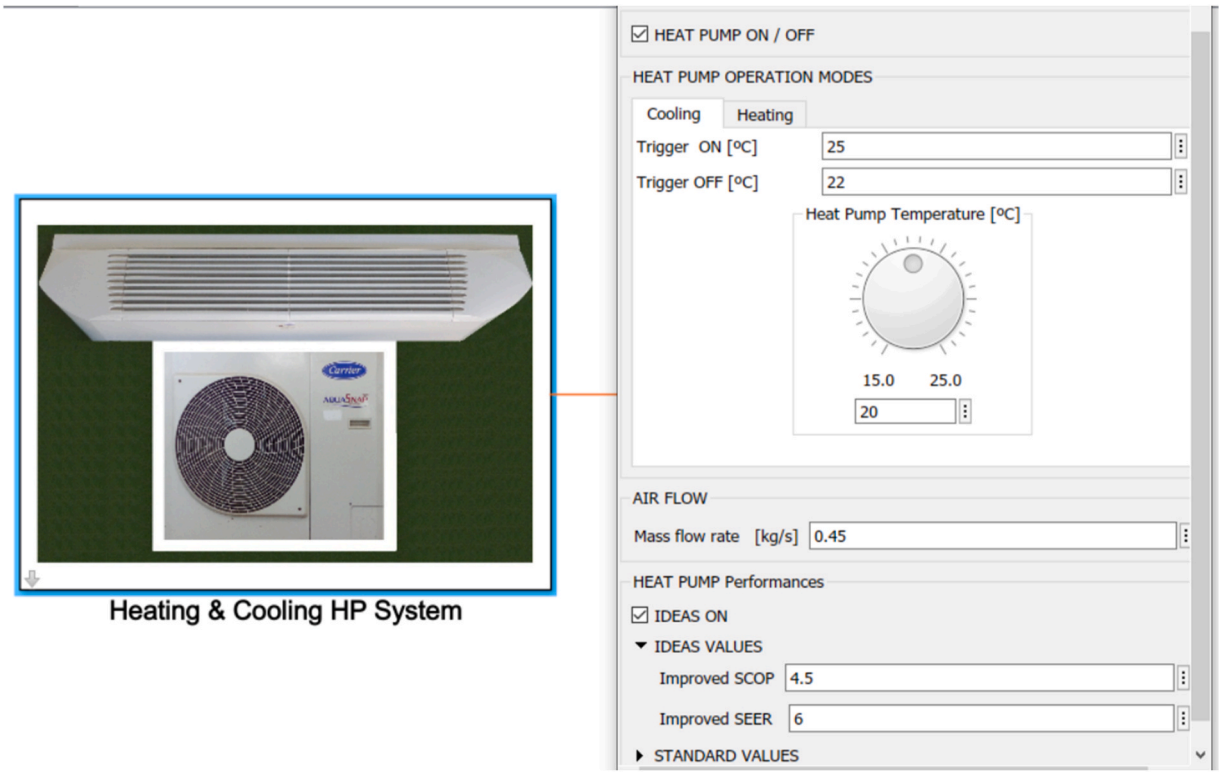

Fig. 20. IDEAS heating & cooling menu.

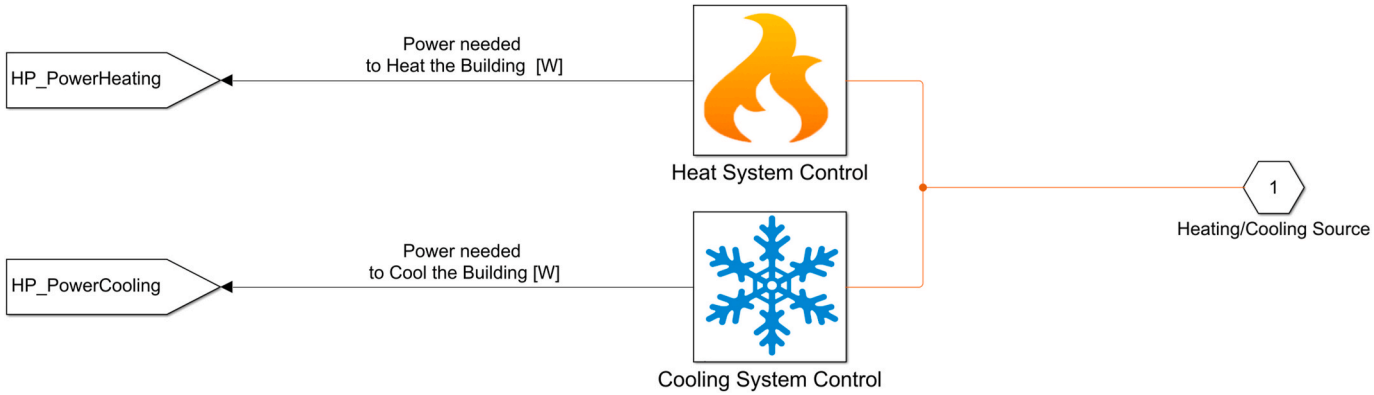

Fig. 21. IDEAS Heating & Cooling HP components.

shown in Equation (9) it follows that the heat flow through a plane wall, q_{wall}, is given by Equation (10), where L is the wall's width, A is the wall's area and k is the wall's thermal conductivity.

$$R_{thermal} = \frac{T_1 - T_2}{q_{wall}} = \frac{L}{k.A} \quad 9$$

$$q_{wall} = \frac{k.A}{L}.(T_1 - T_2) \quad 10$$

This analogy can be used for all the three heat transfer mechanisms, conduction, convection and radiation as shown by Equations (11) to (15), where $q_{convection}$ and $R_{convection}$ are the convection flow and convection resistance of the surface, $q_{radiaton}$ and $R_{radiation}$ are the heat transfer through radiation and the radiation resistance, $T_{surface}$ and $T_{surrounding}$ are the surface and the surface surrounding temperatures, ε is the emissivity of the surface $\in [0,1]$, σ is the Stefan-Boltzmann constant ($5.67 \times 10^{-8}\,Wm^{-2}K^{-4}$), h is the convective heat transfer coefficient and h_r is the radiative heat transfer coefficient.

$$q_{convection} = h.A.\left(T_{surface} - T_{surrounding}\right) \quad 11$$

$$R_{convection} = \frac{T_{surface} - T_{surrounding}}{q_{convection}} = \frac{1}{h.A} \quad 12$$

$$q_{radiation} = h_r.A.\left(T_{surface} - T_{surrounding}\right) \quad 13$$

$$h_r = \varepsilon.\sigma.\left(T_{surface} + T_{surrounding}\right).\left(T^2_{surface} + T^2_{surrounding}\right) \quad 14$$

$$R_{radiation} = \frac{T_{surface} - T_{surrounding}}{q_{radiation}} = \frac{1}{h_r.A} \quad 15$$

The models for the building consider the following gains: air leakage, direct solar gains through the windows, the occupancy (people on average living inside the building) and the heat released by the electric appliances. Regardless of the activity, each person produces an average power of 50 W and for the heat generated by the appliances, it is

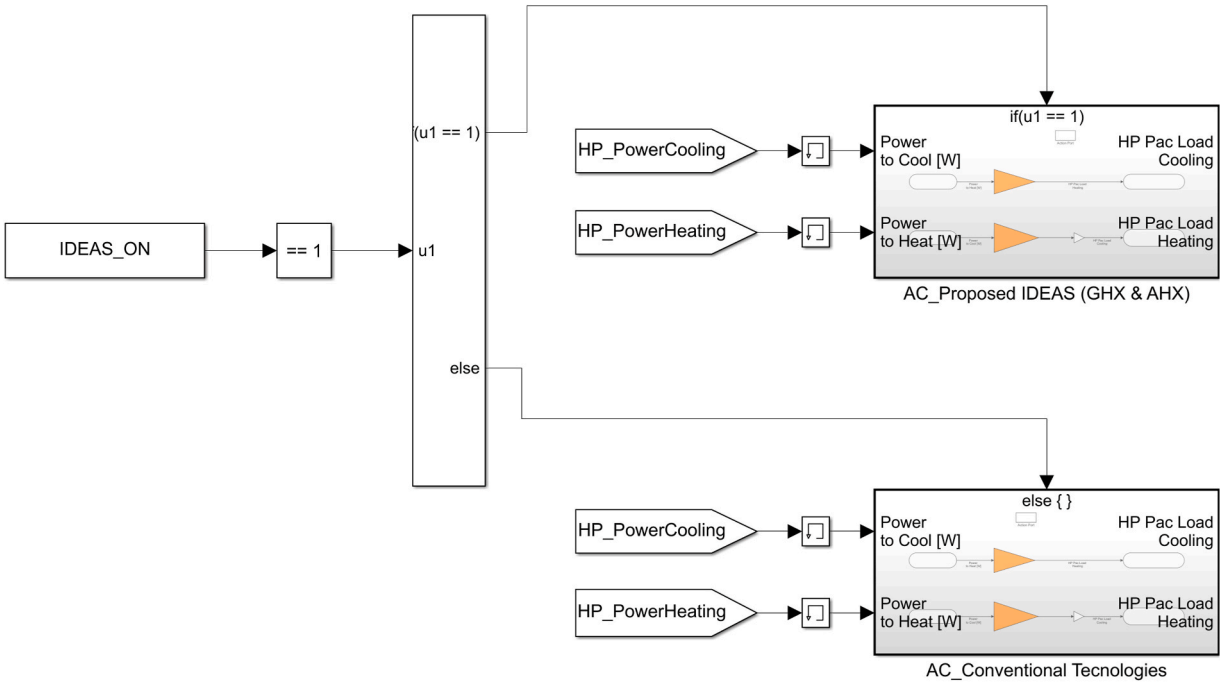

Fig. 22. IDEAS Heating & Cooling HP power calculations.

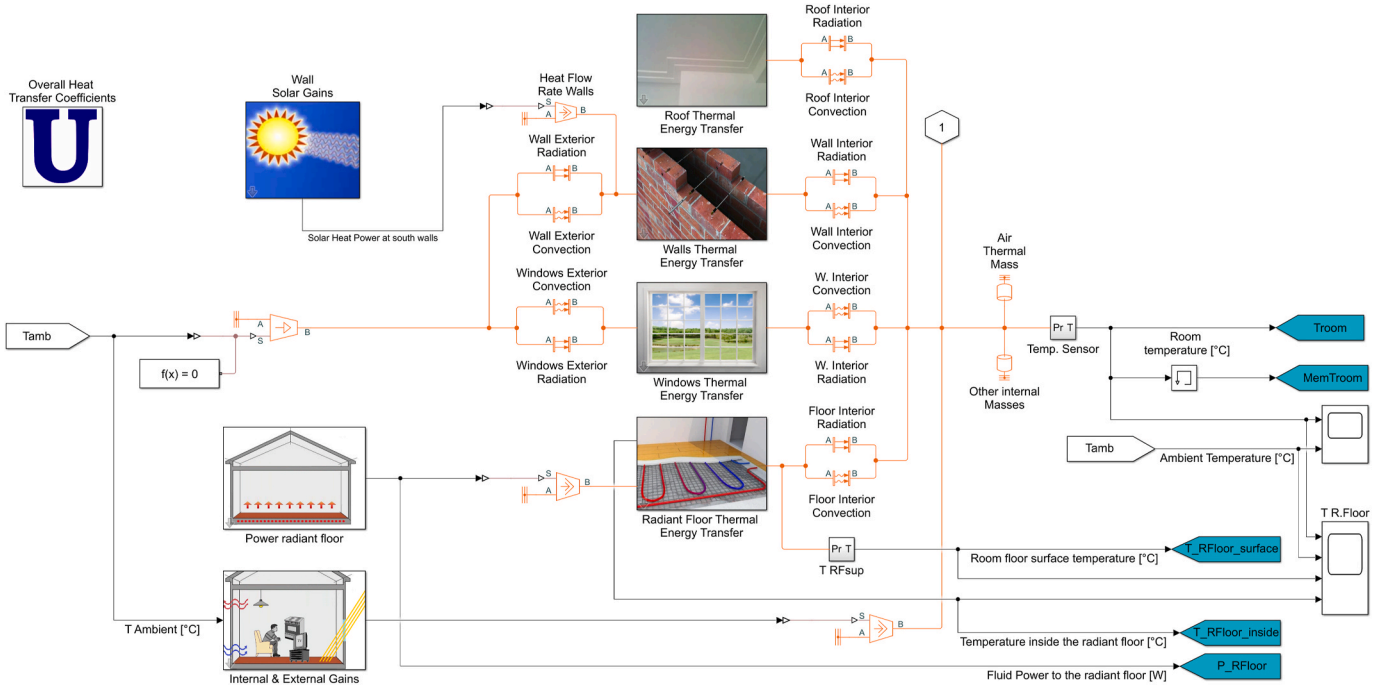

Fig. 23. Building System – considers the energy transfer by conduction and convection with the walls and windows.

Table 5
Calculated Building Heat transfer coefficients (U).

Household building part	U [W/(m^{2}K)]
Walls	0.264
Windows	1.085
Whole building envelope	0.308

assumed that all the energy consumed is converted to heat that remains inside the building. The model also considers the gains from the thermal storage losses if the storage tank is installed inside the building.

The model uses the air renovation rate in Equation (16) to calculate the amount of thermal power lost or gained by the house, $P_{air\ in/out}$, where $Air_{renovation}$ is the air renovation rate, V_{house} is the volume of the house, ρ_{air} is the air density, $c_{p\ air}$ is the specific heat of air and ΔT is the temperature gradient.

$$P_{air\ in/out} = Air_{renovation}.V_{house}.\rho_{air}.c_{p\ air}.\Delta T \quad (16)$$

The direct solar gains through the windows are a function of the incident radiation on the windows, the area of windows facing south, the percentage of glass of the window area, through which direct radiation can pass through, and finally, the absorption coefficient of the glass.

The Building subsystem (Fig. 23) also contemplates a Thermal Radiant Floor system so that the stored solar thermal energy can also be used for heating. Nevertheless, in order to give priority to the use of solar energy stored at the TES, the radiant floor starts first, then the heat pump starts but only works if the temperature of the middle layer of TES is 5 °C higher than the temperature of the bottom layer, and higher than the returned fluid from the radiant floor. The radiant layer in the floor is the layer that comes after the insulation layer and corresponds to the whole structural slab. The radiant floor subsystem's mask is shown in Fig. 24 and the subsystem is depicted in Fig. 25.

2.4. Techno-economic analysis

A simplified techno-economical evaluation of the novel Omega system installed in a household building was developed to analyze the economic benefits. The system cost effectiveness was estimated based on necessary initial investment, operation and maintenance (O&M) costs, cost of fuel (if applicable) and cost of capital. As a result, relevant key economic indicators such as, Levelized Cost of Energy (LCOE), Net Present Value (NPV), Internal Rate of Return (IRR) etc., were assessed using Equations (17)–(20).

2.4.1. Net present value

Net present value can be calculated as follows:

$$NPV = \sum_{t=1}^{n} \frac{S_t}{(1+i)^t} + \frac{RV_n}{(1+i)^n} - I_t \quad (17)$$

where S_t is the cash flow of the system in year t, i the discount rate, t the time, RV_n the residual value, n the operating life time of the Omega system, and I_t the cost of the investment. If the net present value is positive, the investment is financially viable.

2.4.2. Internal rate of return

The internal rate of return (IRR) is used to estimate the profitability of the investment when the NPV is zero. If the IRR is higher than the reference interest rate, the investment is financially viable. The internal rate of return is given as follows:

$$\sum_{t=1}^{n} \frac{S_t}{(1+r)^t} + \frac{RV_n}{(1+r)^n} - I_t = 0 \quad (18)$$

where r is the internal rate of return, and the investment is considered viable when $r \geq i$

A discounted payback period gives the time in years that is needed for the investment to liquidate the invested capital. The discounted payback period is calculated as follows:

$$\sum_{t=1}^{n^*} \frac{S_t}{(1+i)^t} - I_t = 0 \quad (19)$$

where n^* is the payback time. The investment is financially viable if the payback time is lower than the expected lifetime of the investment.

2.4.3. Levelized cost of energy

The levelized cost of energy, *LCOE*, is a measure of the average net present cost of energy production for a generating installation over its lifetime and is calculated as follows:

$$LCOE = \frac{\sum_{t=1}^{n} \frac{I_t + M_t + F_t}{(1+i)^t}}{\sum_{t=1}^{n} \frac{E_t}{(1+i)^t}} \quad (20)$$

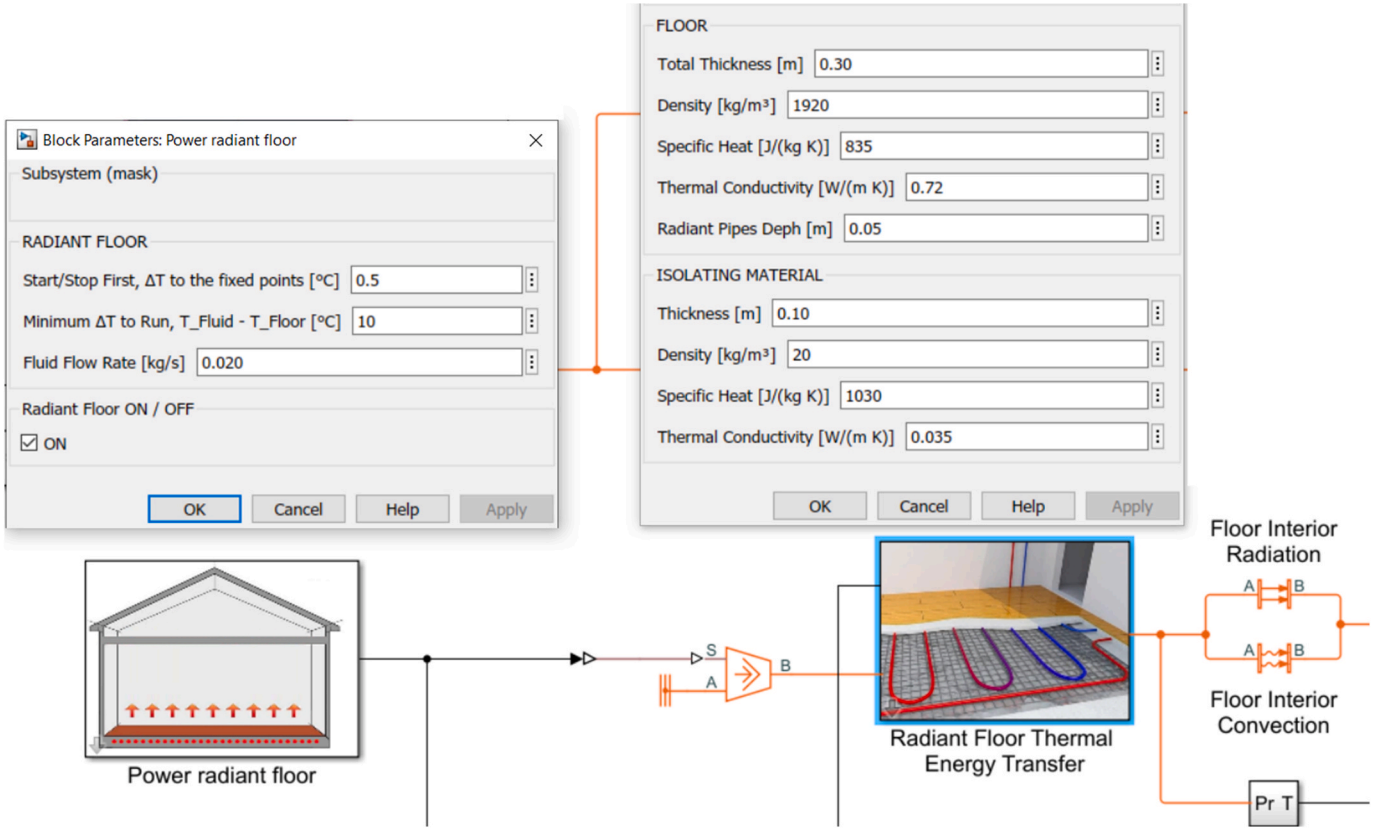

Fig. 24. Power Radiant Floor blocks and related parameters.

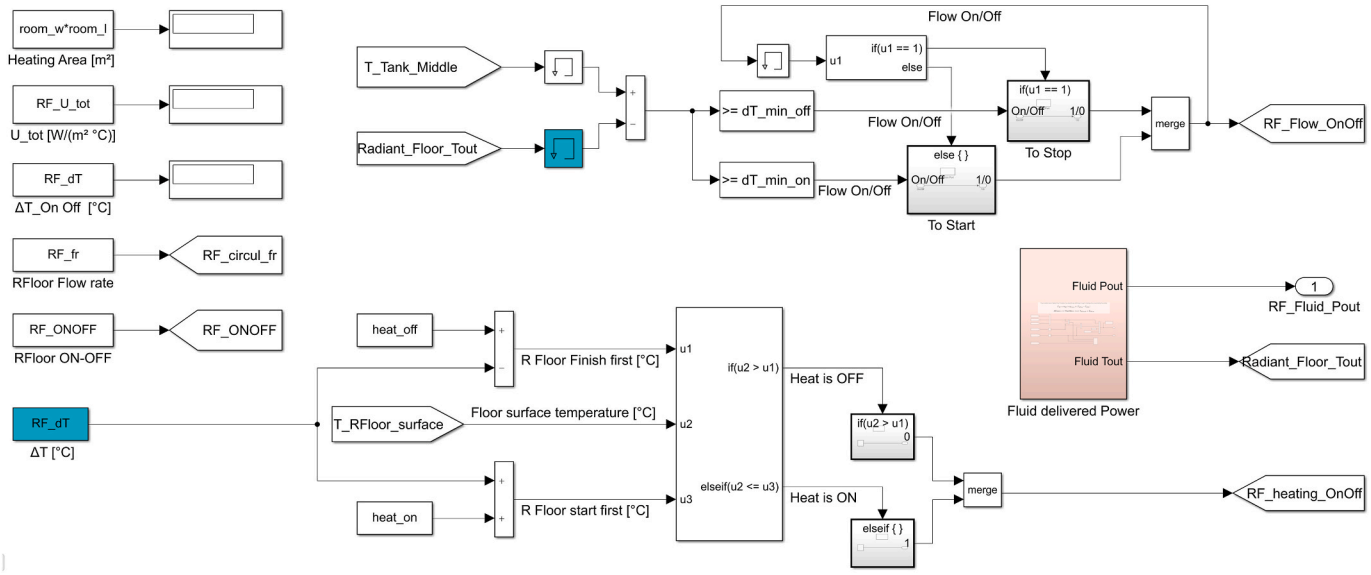

Fig. 25. Power Radiant Floor subsystem.

Where:

I_t: investment expenditures in the year t
M_t: operation and maintenance expenditures in the year t
F_t: fuel expenditures in the year t
E_t: energy (thermal and electric) generated in the year t
i: discount rate
n: expected lifetime of system

Regarding the system expected lifetime, according to Moser et al. [62], the PV module power output might be too low to be economically viable, even though the PV module is still generating power. For economic viability of PV projects, most of the PV module manufacturers, guarantee a power reduction of less than 20 %, referenced at standard test conditions (STC) within 25 years of operation. In the manufacturers' context, the lifetime of a PV module is often defined as the time required for a PV module to lose its initial STC power by 20 % (so-called degradation limit).

3. Results

In this section the numerical results of the Omega system analysis are presented. Firstly, the numerical model was validated with the experimental results from the testing facility in Ferrara. Once validated, the numerical model was used for the performance analysis of the prototype and the contribution to the energy balance of the household, taking into consideration three different locations. In the last part the techno-economic analysis results are presented.

3.1. Experimental validation

The numerical model of Omega system was validated with the experimental results collected in the Ferrara experimental facility. For comparison, measured data from the installed and tested prototype in Ferrara are presented together with simulation results, for two different days, one in winter - January, Fig. 26 (a) and the other in summer - September, Fig. 26 (b).

As it can be observed, the numerical model of the PV power produced by the Omega system, as function of the irradiance, solar height and solar azimuth associated with the CPC geometry, tracks the power produced by the prototype under real conditions.

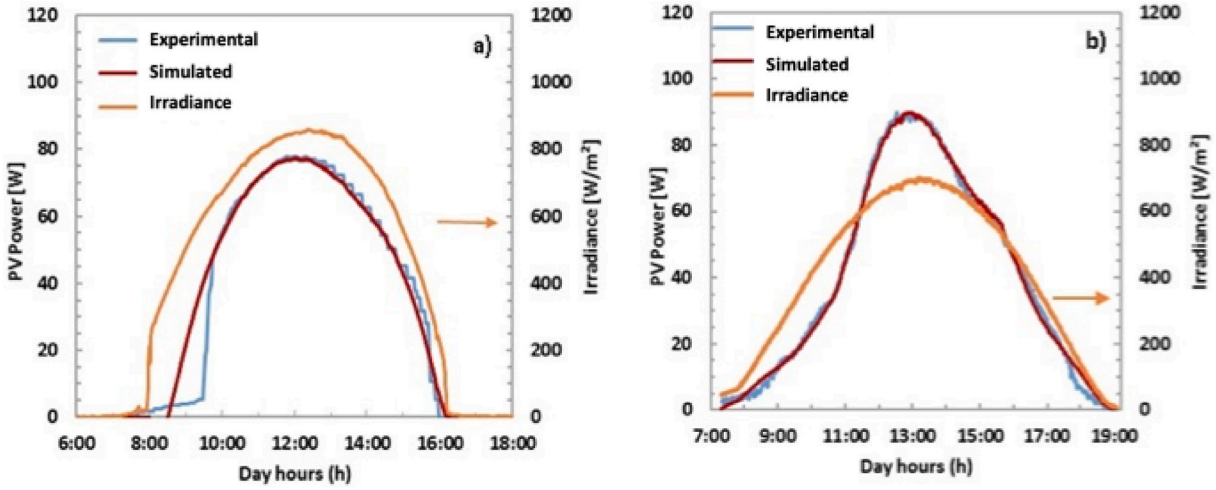

Fig. 26. Model validation results: Power output of Omega system and Irradiance versus day hours on (a) 14-01-2022 and (b) 05-09-2021.

3.2. Performance and use of energy produced

The validated transient model was used to calculate the contribution of the solar energy generated by the Omega System to the energy balance of the building. The simulations were carried out taking in consideration three different locations, Lisbon, Ferrara and Dublin.

To understand the results of the yearly simulation of the building household's use of energy produced, Equations (21)–(26) must be considered.

3.2.1. Thermal energy needs of domestic hot water (DHW)

$$E_{DHW} = E_{solar\ DHW} + E_{AC\ backup\ DHW} \quad (21)$$

where E_{DHW} is the total energy needed to heat the mainswater in order to satisfy the consumption of water at 50 °C, $E_{\mathrm{solar\ DHW}}$ is the total amount of solar thermal energy used and $E_{\mathrm{AC\ backup\ DHW}}$ is the total AC backup electricity used to heat the water from the storage tank, when its temperature is lower than 50 °C.

3.2.2. AC eletrical energy needs supply

$$E_{AC\ loads} + E_{AC\ HP} + E_{AC\ backup\ DHW} = E_{AC\ solar} + E_{AC\ grid} \quad (22)$$

where $E_{\mathrm{AC\ loads}}$ is the AC electricity consumed by load appliances, $E_{\mathrm{AC\ HP}}$ is the AC electricity used by the heat pump, $E_{\mathrm{AC\ solar}}$ is the solar energy converted to AC electricity, and $E_{\mathrm{AC\ grid}}$ is the electricity from the grid.

3.2.3. Total building energy used

$$E_{total} = E_{AC\ loads} + E_{solar\ DHW} + E_{AC\ backup\ DHW} + E_{AC\ HP} + E_{solar\ RF} \quad (23)$$

where E_{total} is the total energy used in the building, and $E_{\mathrm{solar\ RF}}$ is the solar thermal energy used for climatization in the radiant floor.

3.2.4. Total solar energy used (electric and thermal)

$$E_{solar\ used} = E_{AC\ solar} + E_{solar\ DHW} + E_{solar\ RF} \quad (24)$$

where $E_{\mathrm{solar\ used}}$ is the total solar energy (thermal and electric) used in the building.

3.2.5. Solar fraction

$$f_{solar} = E_{solar\ used}/E_{total} \quad (25)$$

where f_{solar} is the fraction of solar energy used.

3.2.6. Global efficiency of the system

$$\eta_{solar} = E_{solar\ used}/E_{solar\ modules} \quad (26)$$

where η_{solar} is the global efficiency of the Omega system.

The results of the contribution of the solar energy generated by the Omega System to the energy balance of the building are presented in Table 6 and represent the solar thermal energy used by the DHW (Solar En. to DHW), the backup energy needed by the DHW (Energy BackUp), the solar energy used by the radiant floor, the thermal losses of the Omega system and TES losses. In the same table, are also shown the Omega system generated electricity used by the Heat Pump (En. Heat Pump) to satisfy the heating and cooling needs, and the appliances load consumption (En. AC loads). Other results shown are the total building energy used, the total amount of solar energy used (thermal and electric), the solar fraction and the global efficiency of the system. It should be noted that the fraction of the solar energy used for the consumption (Solar Fraction) for the IDEAS system presented is higher in Lisbon with 25.9 % while the solar fraction in Ferrara is 16.3 % and in Dublin is 13.8 %. The obtained global efficiency (used energy/incident solar energy) for the three locations is very similar with values of 8.3 %, 8.4 % and 8.9 % respectively. As regards photovoltaic performance conversion, it should be noted that the estimated yearly final yields (useful AC energy/PV STC power installed), are 899 kWh/kW in Lisbon, 713 kWh/kW in Ferrara and 625 kWh/kW in Dublin.

Regarding the performance of the Omega system, the annual production profiles of the Omega system installed at building façades for three different locations Lisbon, Dublin and Ferrara are presented in Figs. 27–29. The line in green shows the available solar energy radiation that reaches the photovoltaic cells after concentration by the CPC. The line in orange represents the thermal energy available to be absorbed by the PCM and the line in blue shows the electrical energy in AC produced by the photovoltaic system and delivered to the electrical grid.

The graphs illustrate the different solar energy availability between cities, resulting from the different weather conditions. Lisbon, with an annual solar energy of 14604 kWh incident on Omega collectors presents the most regular yearly profiles of solar energy on solar cells and electric and thermal energy produced, Fig. 27. Due to the nebulosity, Dublin, with an annual solar energy of 9634 kWh on Omega collectors, presents the most irregular yearly profiles of solar energy incident on solar cells and electric thermal energy produced, Fig. 29.

3.3. Economic analysis

Taking into account the results and energy balance parameters presented previously (Table 4), the estimated costs and benefits corresponding to the integration of the IDEAS system in a typical household located in Lisbon, Ferrara and Dublin are presented in Fig. 30.

The installation of the IDEAS system in Lisbon, with a total estimated yearly use of the solar energy of 1215 kWh and an energy sold to the grid of 40.6 kWh, results on a profit of 266 €. In Ferrara, with a total estimated yearly use of the solar energy of 967 kWh and an energy sold to the grid of 19.8 kWh, results on a profit of 229 €. In Dublin, with a total estimated yearly use of solar energy of 862 kWh and an energy sold to the grid of 20.5 kWh, results on annual profit of 257 €.

3.4. Techno-economic analysis and indicators

Taking into account the base cost values assumed for the Omega system components, two alternative scenarios were considered for the case of system industrialization and production. The economic analysis of the systems can change depending on the scale and the costs of the production. Considering the hypothesis of economies of scale when scaling up the prototypes for industrial manufacturing, two scenarios were considered, (a) considering 50 % of the base cost of the prototype and (b) considering 33 % of the base cost of the prototype (Table 7).

Other components working with Omega system (Table 8) household

Table 6
Numerical results of the energy balance of the household on a yearly basis for Lisbon, Ferrara and Dublin.

Location	Solar En. Module [kWh]	Solar En. to DHW [kWh]	Energy BackUp [kWh]	Radiant Floor [kWh]	Energy OmegaAC [kWh]	En. AC to Heat Pump [kWh]	En. AC to Loads [kWh]	Total En. Used [kWh]	Solar En. Used [kWh]	Solar Fraction	Global Eff.
Lisbon	14 604	607	1019	129	479	289	2650	4693	1215	0.259	0.083
Ferrara	11 458	553	1184	39	376	1512	2650	5936	967	0.163	0.084
Dublin	9634	480	1471	73	309	1580	2650	6254	862	0.138	0.089

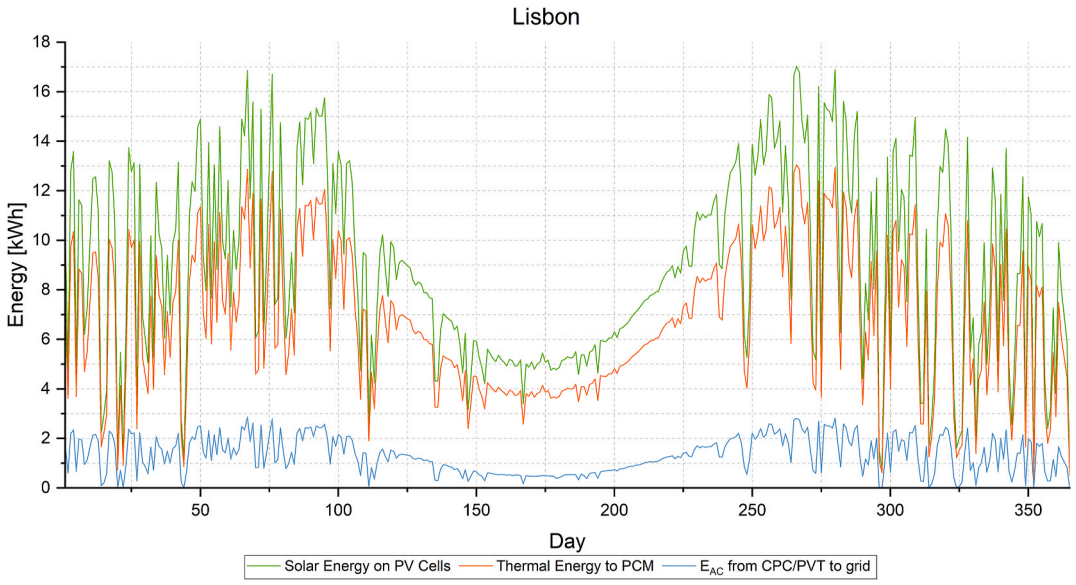

Fig. 27. Results of the annual performance of each component of the Omega system located in Lisbon: energy at PV cells, thermal energy to PCM and AC energy from Omega to the grid.

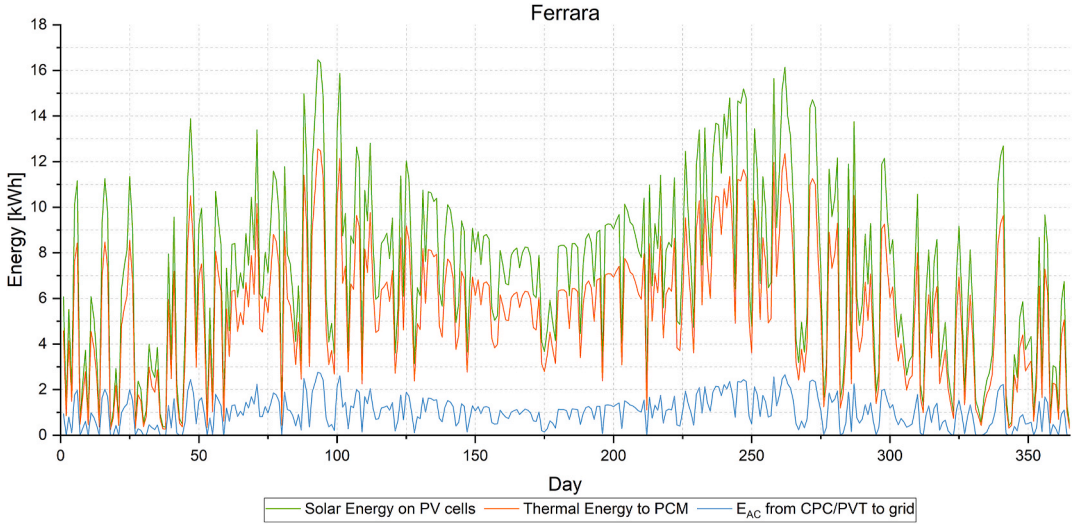

Fig. 28. Results of the annual performance of each component of the Omega system located in Ferrara: energy at PV cells, thermal energy to PCM and AC energy from Omega to the grid.

system were considered in the economic analysis, such as the inverters adapted to the PV power installed with Pac = 0.8 kW, other necessary connections and a thermal storage tank with a capacity of 600 L.

Considering that with mass production this type of PVT module system costs could be highly reduced, Scenario (a) would have an investment cost of 7382 € and Scenario (b) an investment cost of 5918 €.

A financial analysis was developed in order to calculate the main investment feasibility indicators for each variant and scenario under study. The assumptions considered in this analysis are:

- Initial investment costs are the capital applied in the acquisition and implementation of the equipment necessary for the conversion and storage of the energy produced;
- It is considered that this investment is made in the deployment phase of the systems, summarized for the purposes of analysis to the year "0". This assumption restricts the financial viability analysis to the years of effective operation of the systems;
- The expected annual revenues represent the value of the replaced operating costs, i.e. the average cost of the kWh of electricity purchased from the grid, multiplied by the total amount of solar energy produced (thermal and electric) that is self-consumed; plus the revenues from the sale of excess energy to the grid;
- For the purposes referred in the previous paragraph, medium-sized electricity household consumers were considered. In the second semester of 2021, the average electricity retail price reported by Eurostat [63] was in Portugal 0.2170 €/kWh, in Ireland 0.2974 €/kWh and in Italy 0.2360 €/kWh. The constant value of 0.0500 €/kWh was considered as the price of the energy sold to the grid;
- Accounting for the market values and the characteristics of the systems, the initial investments considered for a Household building are presented at Table 7.
- The average annual operation and maintenance costs of the entire system, including the substitution of components, are considered to be 1.0 % of the initial investment value, plus the cost associated with the replacement of the inverters (evaluated at 250 €/kW) at year 10;

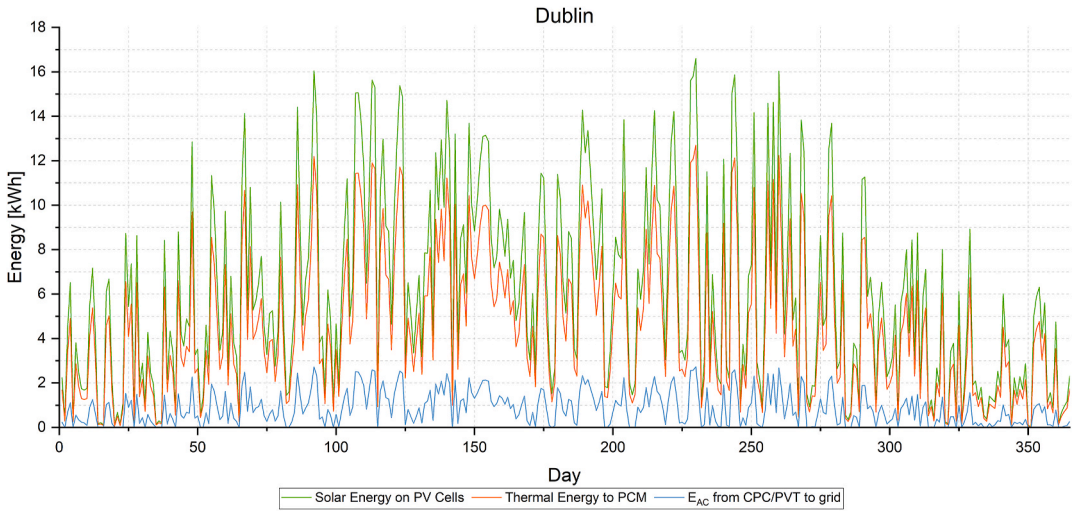

Fig. 29. Results of the annual performance of each component of the Omega system located in Dublin: energy at PV cells, thermal energy to PCM and AC energy from Omega to the grid.

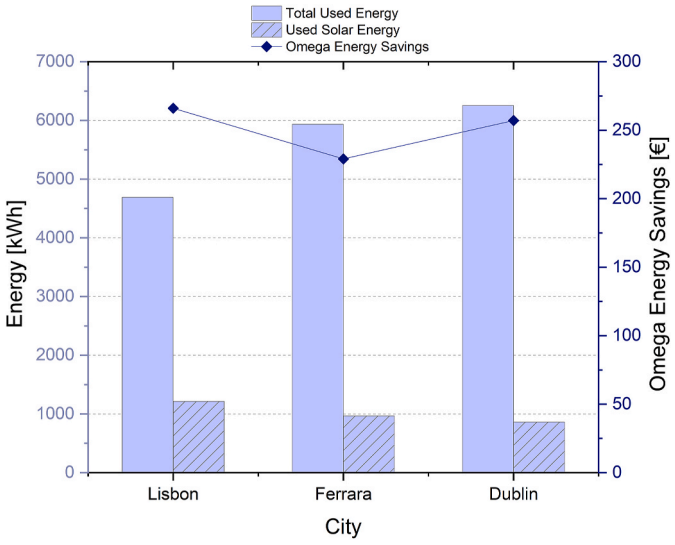

Fig. 30. Results of the household yearly costs and savings with the Omega system for 3 locations.

Table 7
Omega prototype cost & estimation of costs for commercial production [€].

Omega	Cost	Scenario (a)	Scenario (b)
PV Solar cells	174.0	87.0	58.0
CPC Reflector	352.0	176.0	117.0
Frame collector	338.0	169.0	113.0
Thermal absorption	404.0	202.0	135.0
Thermal PCM	194.0	97.0	64.0
Cost Omega	1462.0	731.0	487.0

Table 8
Omega system - Estimation of investment costs at commercial production [€].

Omega system	Scenario (a)	Scenario (b)
Omega prototype	731	487
Thermal storage tank	2196	2196
Inverters	200	200
Other per collector	100	100
Total system (6 collectors)	7382	5918

- For the evaluation of the economic investment decision 3 financial indicators are used, the NPV, IRR and the LCOE for the project lifetime. The simple payback period and the discounted payback period are also indicated at the analysis;
- The assumed discount rate necessary for the calculation of the mentioned indicators was 2.5 %;
- The assumed useful lifetime of the projects is 20 years;
- Costs related to financial charges, amortizations and taxes were not considered.

Household economy results for Lisbon, Ferrara and Dublin considering different scenarios are presented in Table 9 and summarized in Fig. 31.

On the basis of these household economic results, for all the IDEAS Omega system the NPV and IRR indicators present negative values, the discounted payback period is higher than the lifetime of the systems, and the LCOE values are higher than the cost of the electric energy at the second semester of 2021. These results are due to the lower availability of incident solar energy on the collectors installed on façades, relatively to the optimum inclination, typically near 35°. Nevertheless, the price of electricity also can vary over time. In the first semester of 2022 was observed an increase of the price of electricity due to the increase of price of the natural gas by the Russia-Ukraine war. In Italy for example the price of electricity (before all taxes and fees) increased more than 50 %.

4. Discussion

The financial evaluation accounts for the prototype system costs, the expected energy production and savings in energy consumption, and the financial earnings from the sale of surplus energy for each European location. The cost of the Omega PVT prototype, 769.5 €/m^2 (considering a total surface per module of 1.9 m^2) can be compared to a commercial PVT module, 225 €/m^2 [48]. Although there is a great difference in cost, the prototype has innovative features when compared to a commercial PVT module, such as, CPC concentration, PCM in the back of the PV cells for enhanced heat transfer and LDS coating applied on the PV cells top surface to increase the capture of solar radiation.

The numerical model developed for assessing the energy performance of the prototype, was validated with data measured and results were presented for three different European locations. For the system presented, the estimated fraction of the solar energy used for consumption is higher in Lisbon with 25.9 %, while the solar fraction in Ferrara is 16.3 % and in Dublin is 13.8 %. Due to the differences on the

Table 9
Household economic results for the different scenarios and components for Lisbon, Ferrara and Dublin.

Household Building	Lisbon	Ferrara	Dublin	Lisbon	Ferrara	Dublin
Scenario	Scenario (a)			(Scenario (b)		
Annual energy consumption [kWh]	4693	5936	6254	4693	5936	6254
Solar Energy Used [kWh]	1215	967	862	1215	967	862
AC annual production [kWh]	479	376	309	479	376	309
AC Energy from the grid [kWh]	3509	4962	5376	3509	4962	5376
AC Energy to the grid [kWh]	41	20	21	41	20	21
Price of Energy from grid [€/kWh]	0.2170	0.2360	0.2974	0.2170	0.2360	0.2974
Average annual benefits [€]	265.6	229.2	257.3	265.6	229.2	257.3
Initial Investment [€]	7382	7382	7382	5918	5918	5918
Net Present Value [€]	−4123	−4698	−4254	−2428	−3003	−2559
Internal Rate of Return [%]	−5.2 %	−6.7 %	−5.5 %	−2.7 %	−4.3 %	−3.1 %
Levelized cost of energy [€/kWh]	0.322	0.410	0.458	0.260	0.330	0.369

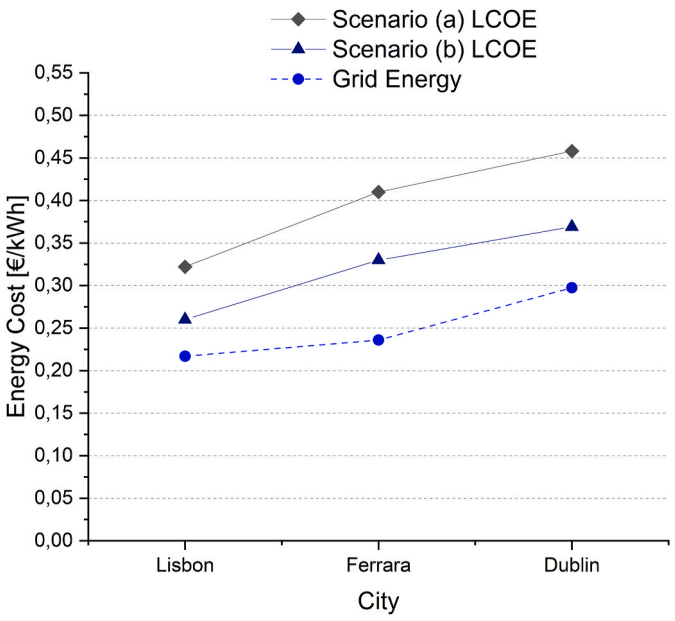

Fig. 31. Comparison of the LCOE for scenario (a) and (b) with the grid electricity price for the 3 countries.

electricity retail price in the countries, installing the system in Lisbon, with a total estimated yearly use of the solar energy of 1215 kWh, results in gains of 266 €, while installing it in Ferrara, with a total estimated yearly use of 967 kWh results in gains of 229 € and in Dublin, with 862 kWh, results in an annual gain of 257 €.

The LCOE values considered for the first scenario are 0.322 €/kWh for Lisbon, 0.410 €/kWh for Ferrara and 0.458 €/kWh for Dublin. These values can be compared to the average thermal energy LCOE for a similar system with 10 m^2 of commercial PVT modules and a thermal storage tank of 1 m^3 in Stuttgart, Germany [47], that was 0.115 €/kWh. The LCOE for the Stuttgart system is much lower, but as stated before, the PVT prototype developed in this work has improvements over a standard flat plate PVT. Also, the orientation and tilt of the Stuttgart system is not stated in Ref. [48], so possibly these parameters are optimized for this location. For trigeneration systems at Bari, Italy, the LCOE was 0.145 €/kWh, but the systems were installed in roofs, could be oriented optimally and tilted with 30° or 10° [47], which increased solar energy captured when compared to a façade system. The obtained LCOE values for both scenarios of system costs are higher than the cost of the electric energy at the second semester of 2021 and are due to the lower availability of incident solar energy on the collectors installed on façades, relatively to the optimum inclination, typically near 35° for these cities. In the first semester of 2022 was observed an increase of the price of electricity due to the increase of price of the natural gas by the Russia-Ukraine war. In Italy for example the price of electricity (before all taxes and fees) increased more than 50 %. In order to lower the LCOE values and facilitate the market entry of this type of multigeneration prototypes, it is advisable that they are also developed for roof installation, where they can be mounted at the optimum inclination and orientation to maximise the capture of solar energy.

The values of the used solar energy in each location are, 1215 kWh for Lisbon, 967 kWh for Ferrara and 862 kWh for Dublin. These values can be converted to find the avoided equivalent CO_2 emissions. Considering that the thermal energy could be produced using an electrical resistance inside the TES, all the produced energy, both thermal and electrical will substitute an electrical consumption. The CO_2 avoided emissions can then be calculated using a CO_2-equivalent for the Portuguese, Italian and Irish power mix of 173 gCO_2eq/kWh, 252 gCO_2 eq/kWh and 315 gCO_2eq/kWh, respectively [64,65]. This leads to 210 $kgCO_2eq$ for Lisbon, 244 $kgCO_2$ eq for Ferrara and 272 $kgCO_2eq$ for Dublin. The average annual avoided emissions for the 3 locations considering the total PVT area for each system, 11.4 m^2, are 21 $kgCO_2eq/m^2$. According to Ref. [8] the annual avoided emissions for multigeneration PVT systems, are 83 $kgCO_2/m^2$. This value is considerably higher than the one obtained for the average of the 3 systems studied in this work, but a possible reason for this difference has already been stated above, when the disadvantages of the integration in façades were discussed.

5. Conclusions and future research

In this paper the authors explore the potential and benefits of a renewable energy based multigeneration prototype using a numerical approach. The prototype is the result of an European research project and integrates a compound parabolic concentrator, a photovoltaic/thermal system with luminescent downshifting layers at PV cells, and thermal storage using phase change materials.

A numerical model was developed for assessing the energy performance of the prototype, validated with data measured and the results are presented for three different European locations. The installation of the IDEAS system in Lisbon, with a total estimated yearly use of solar energy of 1215 kWh and an energy sold to the grid of 40.6 kWh, results on a profit of 266 € (26 % of energy bill). In Ferrara, with a total estimated yearly use of the solar energy of 967 kWh and an energy sold to the grid of 19.8 kWh, results on a profit of 229 € (16 % of energy bill). In Dublin, with a total estimated yearly use of solar energy of 862 kWh and an energy sold to the grid of 20.5 kWh, results on annual profit of 257 € (14 % of energy bill).

A simplified economic analysis was also developed and presented for two different scenarios at the same locations. Due to the lower availability of incident solar energy on the collectors installed on façades, LCOE values are higher than the cost of the electric energy at the second semester of 2021. Nevertheless, due to the recent increase of the price of electricity as a consequence of the war in Ukraine, the installation of

photovoltaic and thermal systems on the façades can be in some countries an affordable way of satisfying part of the energy consumption at households.

As future research, the assessment of the multigeneration prototypes based on the same technologies designed and developed for roof installation, thus maximising the capture of solar use, in order to lower the LCOE values of energy produced will be analysed. Also, the simulation tool that was developed in this work will allow for a sensitivity analysis to be done by changing each factor at a time (orientation, tilt, climatic conditions, etc) and evaluating its impact on the system's productivity. This analysis will allow the identification of which factors have a greater impact in the system's performance and therefore should be prioritized and optimized in new system developments. Moreover, the benefits of using this kind of system will be assessed from the perspective of comfort and indoor air quality, and environmental and climate impact.

CRediT authorship contribution statement

L. Aelenei: Writing – review & editing, Writing – original draft, Project administration, Methodology, Conceptualization. **C. Rodrigues:** Validation, Software, Resources, Investigation, Data curation. **M.J. Brites:** Writing – review & editing, Writing – original draft, Conceptualization. **S. Viana:** Writing – review & editing, Writing – original draft, Visualization, Resources.

Declaration of competing interest

The authors declare the following financial interests/personal relationships which may be considered as potential competing interests: Laura Aelenei reports financial support was provided by National Laboratory for Energy and Geology. If there are other authors, they declare that they have no known competing financial interests or personal relationships that could have appeared to influence the work reported in this paper.

Acknowledgments

This research was carried out in the scope of the project IDEAS-Novel building Integration Designs for increased Efficiencies in Advanced climatically tunable renewable energy Systems, supported by the Horizon2020, H2020-LC-SC3-2018-2019-2020 program under the Grant Agreement [NUMBER 815271].

References

[1] DIRECTIVE (EU) 2024/1275 OF THE EUROPEAN PARLIAMENT AND OF THE COUNCIL of 24 April 2024 on the energy performance of buildings. https://eur-lex.europa.eu/legal-content/EN/TXT/PDF/?uri=OJ:L_202401275. (Accessed 14 November 2024).

[2] European Parliament 'Directive 2010/31/EU of the European Parliament and of the Council of 19 May 2010 on the Energy Performance of Buildings (Recast)' Official Journal of the European Union, 2010; 2010 [Google Scholar].

[3] S. Attia, J. Kurnitski, P. Kosinski, A. Borodinecs, Z.D. Belafi, K. István, H. Krstic, M. Moldovan, I. Visa, N. Mihailov, B. Evstatiev, K. Banionis, M. Cekon, S. Vilceková, Struhala Karel, R. Brzon, O. Laurent, Overview and future challenges of nearly zero-energy building (nZEB) design in Eastern Europe, Energy Build. 267 (2022) 112165, https://doi.org/10.1016/j.enbuild.2022.112165.

[4] L. Aelenei, H. Petran, J. Tarrés, G. Riva, A. Ferreira, S. Camelo, V. Corrado, M. Šijanec-Zavrl, G. Stegnar, H. Gonçalves, Z. Magyar, J. Salom, E. Polychroni, K. Sfakianaki, New challenge of the public buildings: nZEB findings from IEE RePublic_ZEB project, Energy Proc. 78 (2015) 2016–2021, https://doi.org/10.1016/j.egypro.2015.11.195.

[5] R.K. Jaysawal, S. Chakraborty, D. Elangovan, S. Padmanaban, Concept of net zero energy buildings (NZEB) - a literature review, Cleaner Eng. Technol. 11 (2022) 100582, https://doi.org/10.1016/j.clet.2022.100582.

[6] K. Bot, L. Aelenei, M.G. Gomes, C. Santos Silva, A literature review on Building Integrated Solar Energy Systems (BI-SES) for façades – photovoltaic, thermal and hybrid systems, Renew. Energy Environ. Sustain 7 (2022), https://doi.org/10.1051/rees/2021053.

[7] A. Kumar, P. Baredar, U. Qureshi, Historical and recent development of photovoltaic thermal (PVT) technologies, Renew. Sustain. Energy Rev. 42 (2015) 1428–1436, https://doi.org/10.1016/j.rser.2014.11.044.

[8] M. Herrando, K. Wang, G. Huang, T. Otanicar, O. Mousa, R. Agathokleous, Y. Ding, S. Kalogirou, N. Ekins-Daukes, R. Taylor, C. Markides, A review of solar hybrid photovoltaic-thermal (PV-T) collectors and systems, Prog. Energy Combust. Sci. 97 (2023) 101072, https://doi.org/10.1016/j.pecs.2023.101072.

[9] F. Masood, N. Nor, P. Nallagownden, I. Elamvazuthi, R. Saidur, M. Alam, J. Akhter, M. Yusuf, M. Mehmood, M. Ali, A review of recent developments and applications of compound parabolic concentrator-based hybrid solar photovoltaic/thermal collectors, Sustainability 14 (9) (2022) 5529, https://doi.org/10.3390/su14095529.

[10] A. Bouzoukas, New Approaches for Cooling Photovoltaic/Thermal (PV/T) Systems [Internet], [University of Nottingham]: University of Nottingham, 2008. Available from: http://core.kmi.open.ac.uk/display/385947.

[11] K. Pelletier, C. Wood, J. Calautit, Y. Wu, The viability of double-skin façade systems in the 21st century: a systematic review and meta-analysis of the nexus of factors affecting ventilation and thermal performance and building integration, Build. Environ. 228 (2023) 109870, https://doi.org/10.1016/j.buildenv.2022.109870.

[12] J. Taherahmadi, Y. Noorollahi, M. Panahi, Toward comprehensive zero energy building definitions: a literature review and recommendations, Int. J. Sustain. Energy 40 (N°. 2) (2021) 120–148, https://doi.org/10.1080/14786451.2020.1796664.

[13] L. Aelenei, S. Paduos, H. Petran, J. Tarrés, A. Ferreira, V. Corrado, S. Camelo, E. Polychroni, K. Sfakianaki, H. Gonçalves, J. Salom, G. Riva, G. Murano, Implementing cost-optimal methodology in existing public buildings, Energy Proc. 78 (2015) 2022–2027, https://doi.org/10.1016/j.egypro.2015.11.197.

[14] F. Pomponi, et al., Energy performance of Double-Skin Façades in temperate climates: a systematic review and meta-analysis, Renew. Sustain. Energy Rev. 54 (2016) 1525–1536.

[15] S.H. Bandaru, V. Becerra, S. Khanna, J. Radulovic, D. Hutchinson, R. Khusainov, A review of photovoltaic thermal (PVT) technology for residential applications: performance indicators. Progress, and opportunities, Energies 14 (2021) 3853, https://doi.org/10.3390/en14133853.

[16] Noxpanco, M.G., Wilkins, J., Riffat, S. A review of the recent development of photovoltaic/thermal (PV/T) systems and their applications. Future Cities and Environment, 6(1): 9, 1–16. DOI: DOI:10.5334/fce.97.

[17] A.K. Hamzat, A.Z. Sahin, M.I. Omisanya, L.M. Alhems, Advances in PV and PVT cooling technologies: a review, Sustain. Energy Technol. Assessments 47 (2021) 101360, https://doi.org/10.1016/j.seta.2021.101360.

[18] C. Jiao, Z. Li, An updated review of solar cooling systems driven by photovoltaic–thermal collectors, Energies 16 (2023) 5331, https://doi.org/10.3390/en16145331.

[19] B. Petter Jelle, C. Breivik, H. Drolsum Røkenes, Building integrated photovoltaic products: a state-of-the-art review and future research opportunities, Sol. Energy Mater. Sol. Cells 100 (2012) 69–96, https://doi.org/10.1016/j.solmat.2011.12.016.

[20] Y. Cai, Y. Huang, Z. Shu, Z. Liu, H. Zhong, F. Zhao, Investigation of double-PCM based PV composite wall for power-generation and building insulation: Thermal characteristics and energy consumption prediction, Energy and Built Environment (2025), https://doi.org/10.1016/j.enbenv.2024.08.002. In press.

[21] D. Singh, A.K. Gautam, R. Chaudhary, Application of phase change material in building integrated photovoltaics: a review, Mater. Today Proc. 45 (2021) 4624–4628, https://doi.org/10.1016/j.matpr.2021.01.021.

[22] L. Aelenei, H. Gonçalves, From solar building design to net zero energy buildings: performance insights of an office building, Energy Proc. 48 (2014) 1236–1243, https://doi.org/10.1016/j.egypro.2014.02.140.

[23] R. Pereira, L. Aelenei, Optimization assessment of the energy performance of a BIPV/T-PCM system using Genetic Algorithms, Renew. Energy 137 (2019) 157–166, https://doi.org/10.1016/j.renene.2018.06.118.

[24] L. Aelenei, R. Pereira, Innovative solutions for net zero-energy building: BIPV-PCM system - modelling, design and thermal performance IYCE 2013 - 4th, Int. Youth Conf. Energy (2013) 6604162.

[25] L. Aelenei, R. Pereira, H. Gonçalves, A. Athienitis, Thermal performance of a hybrid BIPV-PCM: modelling, design and experimental investigation, Energy Proc. 48 (2014) 474–483, https://doi.org/10.1016/j.egypro.2014.02.056.

[26] L. Aelenei, R. Pereira, A. Ferreira, H. Gonçalves, A. Joyce, Building integrated photovoltaic system with integral thermal storage: a case study, Energy Proc. 58 (2014) 172–178, https://doi.org/10.1016/j.egypro.2014.10.425.

[27] K. Bot, L. Aelenei, M. Da Glória Gomes, C.S. Silva, Performance assessment of a building integrated photovoltaic thermal system in Mediterranean climate - a numerical simulation approach, Energies 13 (11) (2020) 2887, https://doi.org/10.3390/en13112887.

[28] J.M. Lourenço, L. Aelenei, M. Sousa, J. Facão, H. Gonçalves, Thermal behavior of a BIPV combined with water storage: an experimental analysis, Energies 14 (9) (2021) 2545, https://doi.org/10.3390/en14092545.

[29] B.S. Richards, The performance of silicon solar cells via the application of passive luminescence conversion layers, Sol. Energy Mater. Sol. Cells 90 (2006) 2329–2337.

[30] B. McKenna, R.C. Evans, Towards efficient spectral converters through materials design for luminescent solar devices, Adv. Mater. 29 (2017) 1606491.

[31] E. Klampaftis, D. Ross, K.R. McIntosh, B.S. Richards, Enhancing the performance of solar cells via luminescent down-shifting of the incident spectrum: a review, Sol. Energy Mater. Sol. Cells 93 (2009) 1182–1194.

[32] M.G. Debije, P.P.C. Verbunt, Thirty years of luminescent solar concentrator research: solar energy for the built environment, Adv. Energy Mater. 2 (2012) 12–35.
[33] R. Fernandes, N. Bristow, V. Stoichkov, H. Anizelli, J. Duarte, E. Laureto, J. Kettle, Development of multidye UV filters for OPVs using luminescent materials, J. Phys. Appl. Phys. 50 (Number 2) (2017) 025103, https://doi.org/10.1088/1361-6463/50/2/025103.
[34] A. Farooq, I. Hossain, S. Moghadamzadeh, J. Schwenzer, T. Abzieher, B. Richards, E. Klampaftis, U. Paetzold, Spectral dependence of degradation under ultraviolet light in perovskite solar cells, ACS Appl. Mater. Interfaces 10 (26) (2018) 21985–21990, https://doi.org/10.1021/acsami.8b03024.
[35] E. Klampaftis, B.S. Richards, Improvement in multi-crystalline silicon solar cell efficiency via addition of luminescent material to EVA encapsulation layer, Prog. Photovoltaics Res. Appl. 19 (2011) 345–351.
[36] S.A. Sadhu, Y.M. Huang, L.Y. Chen, H.C. Kuo, C.C. Lin, Recent advances in colloidal quantum dots or perovskite quantum dots as a luminescent downshifting layer embedded on solar cells, Nanomaterials 12 (2022) 98.
[37] M. Hong, T. Xuan, J. Liu, Z. Jiang, Y. Chen, X. Chen, H. Li, Air-exposing microwave-assisted synthesis of $CuInS_2$/ZnS quantum dots for silicon solar cells with enhanced photovoltaic performance, RSC Adv. 5 (2015) 102682–102688.
[38] Y. Nakamura, Y. Iso, T. Isobe, Bandgap-tuned $CuInS_2$/ZnS core/shell quantum dots for a luminescent downshifting layer in a crystalline silicon solar module, ACS Appl. Nano Mater. 3 (2020) 3417–3426.
[39] L. Meng, X.G. Wu, S. Ma, L. Shi, M. Zhang, L. Wang, Y. Chen, Q. Chen, H. Zhong, Improving the efficiency of silicon solar cells using in situ fabricated perovskite quantum dots as luminescence downshifting materials, Nanophotonics 9 (1) (2020) 93–100.
[40] J. Liu, K. Wang, W. Zheng, W. Huang, C.H. Li, X.Z. You, Improving spectral response of monocrystalline silicon photovoltaic modules using high efficient luminescent down-shifting Eu^{3+} complexes, Prog. Photovoltaics Res. Appl. 21 (2013) 668–675.
[41] Jakica N, Kragh M, Rebecca J. Pabasara YWM, Wijeratne U, Too E, Wakefield R, Eisenlohr J, Boddaert S, Bonomo P, Saretta E, Frontini F, Zanelli A, Freitas S, Alamy P, Leloux J. BIPV design and performance modelling: tools and methods. Report IEA-PVPS T15-09:2019.
[42] https://iea-pvps.org/wp-content/uploads/2020/01/IEA-PVPS_15_R09_BIPV_Design_Tools_report.pdf.
[43] A. Jain, R. Mehta, S.K. Mittal, Modeling impact of solar radiation on site selection for solar PV power plants in India, Int. J. Green Energy 8 (4) (2011) 486–498.
[44] K.K. Shah, A.S. Mundada, J.M. Pearce, Performance of U.S. hybrid distributed energy systems: solar photovoltaic, battery and combined heat and power, Energy Convers. Manag. 105 (2015) 71–80.
[45] T. Roberts, N. Stace, A. Roberts, D. Conway, J.V. Van Nettern, N. Woodard, Moving your campus Smartly to 100% renewable energy, in: Proceedings of the 16th International Australasian Campuses towards Sustainability (ACTS) Conference, Sunshine Coast, Australia, 2016.
[46] C.P. Cameron, W.E. Boyson, D.M. Riley, Comparison of PV system performance-model predictions with measured PV system performance, in: Photovoltaic Specialists Conference, PVSC '08. 33rd IEEE, 2008, pp. 1–6.
[47] M. Herrando, A.M. Pantaleo, K. Wang, C.N. Markides, Solar combined cooling, heating and power systems based on hybrid PVT, PV or solar-thermal collectors for building applications, Renew. Energy 143 (2019) 637–647, https://doi.org/10.1016/j.renene.2019.05.004.
[48] R. Braun, M. Haag, J. Stave, N. Abdelnour, U. Eicker, System design and feasibility of trigeneration systems with hybrid photovoltaic-thermal (PVT) collectors for zero energy office buildings in different climates, Sol. Energy 196 (2020) 39–48, https://doi.org/10.1016/j.solener.2019.12.005.
[49] Soursos Bakos, Tsagas.Techno economic assessment of a building-integrated PV system for electrical energy saving in residential sector, Energy Build. 35 (8) (2003) 757–762.
[50] A. Joyce, L. Coelho, J.F. Martins, N. Tavares, R. Pereira, P. Magalhães, A PV/T and heat pump based trigeneration system model for residential applications, in: Proceedings of the ISES Solar World Congress, Kassel, Germany, 28 August–2 September 2011. https://repositorio.lneg.pt/bitstream/10400.9/1355/1/ISES_SWC_2011_Paper_40892.pdf.
[51] S. Reichelstein, M. Yorston, The prospects for cost competitive solar PV power, Energy Policy 55 (2013) 117–127.
[52] S. Rehman, M.A. Bader, S.A. Al-Moallem, Cost of solar energy generated using PV panels, Renew. Sustain. Energy Rev. 11 (8) (2007) 1843–1857.
[53] C. Good, I. Andresen, A.G. Hestnes, Solar energy for net zero energy buildings – a comparison between solar thermal, PV and photovoltaic–thermal (PV/T) systems, Sol. Energy 122 (2015) 986–996.
[54] A. Ghafoor, A. Munir, Design and economics analysis of an off-grid PV system for household electrification, Renew. Sustain. Energy Rev. 42 (2015) 496–502.
[55] K.J. Sauer, T. Roessler, C.W. Hansen, Modeling the irradiance and temperature dependence of photovoltaic modules in PVsyst. Photovoltaics, IEEE Journal 5 (1) (2015) 152–158.
[56] K. Hang-Jung, H. Shang-Hsien, G. Rong-Chin, C. Chi-Chang, A verification study for energy analysis of BIPV buildings with BIM, Energy Build. 130 (2016) 676–691.
[57] R. Brauna, M. Haagb, J. Staveb, N. Abdelnourb, U. Eicker, System design and feasibility of trigeneration systems with hybrid photovoltaic-thermal (PVT) collectors for zero energy office buildings in different climates, Sol. Energy 196 (2020), https://doi.org/10.1016/j.solener.2019.12.005, 39–4.
[58] IDEAS project. https://www.horizon2020ideas.eu. (Accessed 27 January 2023).
[59] D. Faiman, Assessing the outdoor operating temperature of photovoltaic modules, Prog. Photovoltaics Res. Appl. 16 (4) (2008) 307–315.
[60] M. Koehl, M. Heck, S. Wiesmeier, Categorization of weathering stresses for photovoltaic modules, Energy Sci. Eng. 6 (2) (2018) 93–111.
[61] C.A. Cruickshank, S.J. Harrison, Heat loss characteristics for a typical solar, domestic hot water storage, Energy Build. 42 (10) (2010) 1703–1710, https://doi.org/10.1016/j.enbuild.2010.04.013. ISSN 0378-7788.
[62] D. Moser, S. Lindig, M. Richter, J.A. Vásquez, I. Horvath, B. Müller, M. Green, J. Vedde, M. Herz, B. Herteleer, K.A. Weiß, B. Stridh, Uncertainties in yield assessments and PV LCOE, in: Report IEAPVPS T13-18, IEA-PVPS, 2020. ISBN 978-3-907281-06-2, https://iea-pvps.org/keytopics/uncertainties-yield-assessments/. (Accessed 27 January 2023).
[63] Eurostat - European Commission, Electricity Price Statistics, (Online; accessed: 2022-07-05), https://ec.europa.eu/eurostat/statistics-explained/index.php?title=Electricity_price_statistics.
[64] Greenhouse gas emission intensity of electricity generation in Europe, Euro. Environ. Agency, https://www.eea.europa.eu/en/analysis/indicators/greenhouse-gas-emission-intensity-of-1 [Accessed 25/January/2024].
[65] Carbon emissions of different fuels, https://www.forestresearch.gov.uk/tools-and-resources/fthr/biomass-energy-resources/reference-biomass/facts-figures/carbon-emissions-of-different-fuels/[Accessed: 23/November/2024].